

A Unified Theory for Interphase Transport Phenomena with Interfacial Velocity and Surface Tension Gradients: Applications to Single Crystal Growth and Microgravity Sciences

Akira Hirata¹

Abstract: This article is a summary of author's typical research works (over the last four decades) on interphase transport phenomena in the presence of interfacial fluid motion and surface tension gradients on liquid-fluid interfaces, and related applications to single crystal growth and microgravity sciences. A unified theory for momentum, heat and mass transfer on liquid-fluid and solid-fluid interfaces is proposed, which takes into account interface mobility. It is shown that interface contamination and turbulence can be well explained, respectively, by suppression and enhancement of the interfacial velocity induced by surface tension gradients. Transport phenomena on solid spheres, liquid drops and gas bubbles are also treated within the context of the proposed theory. This theory is then extended to the case of crystal-melt and melt-fluid interfaces. Results provided by microgravity experiments performed with drop shafts, parabolic flights, sounding rockets and the space shuttle are used as a relevant means for further elaboration and validation of the proposed theoretical framework.

Keyword: Transport phenomena, interfacial velocity, surface tension gradient, Marangoni convection, single crystal growth, microgravity experiments, Bridgman method, floating zone method, Czochralsky method.

1 Introduction

Interphase transport phenomena are very important as a fundamental issue for a variety of diffusional operations in chemical and biochemical processes, such as gas absorption and liquid-

liquid extraction. Moreover, these phenomena play an important role in single crystal processing.

Since there are many variables which influence interphase transport phenomena in a complicated manner, however, only few theories were proposed before the 60's to explain the underlying mechanisms (Shirotsuka, Hirata and Murakami, 1966).

From this standpoint, the author worked for 50 years to shed some light on the mechanisms of momentum, heat and mass transfer on solid-fluid and liquid-fluid interfaces, to introduce new theories and extend them to surface-tension-gradient-driven convection phenomena in high quality single crystal growth and microgravity sciences (Hirata, 2005).

The interface mobility, specifically the interfacial fluid motion caused by surface tension gradients, is considered in this study and a unified theory is proposed for the interphase transport phenomena on solid spheres, liquid drops and gas bubbles.

The interface mobility is the most important variable distinguishing interphase transport phenomena between a liquid-fluid interface and a solid-fluid interface. Three important non-dimensional parameters are introduced in such unified theory: the non-dimensional interfacial velocity, the non-dimensional ratio of surface tension gradient driven force to viscous force (or inertia force), and the non-dimensional contamination degree. With the unified theory, interfacial contamination phenomena and interfacial turbulence are well explained, respectively, by suppression and enhancement of the interfacial velocity which are caused by negative and positive surface tension gradients on the liquid-fluid interface, respec-

¹ Waseda University, Tokyo, 169-8555 Japan. Professor A. Hirata passed away on April 13, 2007.

tively.

In bulk single crystal growth from melt by the Bridgman method, the floating zone (FZ) method and the Czochralsky (CZ) method, the crystal quality is influenced strongly by convection in the melt. Early works only considered forced and natural convections. Over recent years, the author has provided some insights into the transport phenomena on the crystal-melt interface and the melt-ambient fluid interface, accounting for surface tension gradient driven convection. As an example, single peaked and high efficiency ultraviolet emission at 345 nm from $\text{In}_{0.03}\text{Al}_{0.20}\text{Ga}_{0.77}\text{N}$ LEDs has been achieved with MOVPE under continuous current injection conditions.

Although it was a widespread opinion before 1990 that no convection existed in microgravity, the author pointed out that the interfacial-tension-gradient-driven convection, or Marangoni convection, could be very important even in microgravity conditions. The mechanism of thermocapillary and solutal convections in two-dimensional open boats and liquid bridges, under both gravity and microgravity conditions was elucidated via microgravity experiments performed with drop shafts, parabolic flights, sounding rockets and the space shuttle, as well as on the ground.

Owing to the large amount of articles published by the author and related results, the present article will be limited to giving some flavor of the most significant results, by showing some examples and by introducing the unified theoretical framework mentioned before. The reader interested in a more thorough discussion should consult the relevant sections of the articles cited hereafter.

2 Transport phenomena with interfacial velocity on solid-fluid interfaces

For the case of transport phenomena with interfacial velocity on solid-fluid interfaces, the reader may consider Hirata & Shiotsuka (1967), Shiotsuka & Hirata (1970), Shiotsuka & Hirata (1967) and Shiotsuka et al. (1969).

In such works, it was made clear quantitatively from both the theoretical and experimental re-

sults that, for the conditions considered therein, the rate of heat transfer with mass transfer decreases against an increase in the mass transfer rate, due to mass transfer cooling, and the effect of the Schmidt number on the mass transfer rate depends on the interfacial velocity, which promotes mass transfer.

3 Transport phenomena on liquid-fluid interface

Interphase transport phenomena on a liquid-fluid interface are influenced by many variables in a manner more complicated than that on solid-fluid stationary interface. The interfacial mobility is the most significant variable in distinguishing interphase transport phenomena between a liquid-fluid interface and a solid-fluid stationary interface. The author has studied interphase transport phenomena on liquid-fluid interface, paying particular attention to this interfacial mobility.

3.1 Transport phenomena in high mass flux mass transfer

Momentum, heat and mass transfer phenomena in a laminar boundary layer on a liquid-fluid interface were theoretically analyzed with tangential and normal interfacial velocities taken into account simultaneously.

Approximate equations governing the effects of tangential and normal interfacial velocities on these phenomena were proposed by Hirata, Kira and Suzuki (1979a), Hirata and Suzuki (1980). The following important results were obtained:

1. The interfacial velocity parallel to bulk stream increases heat and mass transfer rates,
2. The normal velocity to the interface from the bulk stream (such as gas absorption) increases heat and mass transfer rates,
3. The normal velocity to the bulk stream from the interface (such as evaporation) decreases heat and mass transfer rates.

In all cases, it should be pointed out that the effects are more important with larger Schmidt numbers.

3.2 Interphase mass transfer between two planar laminar layers with a flowing interface

Both an experimental and an approximate analysis were made about the effect of the interfacial velocity on interphase mass transfer with a tangentially moving liquid-liquid (immiscible) interface between two plane laminar layers (Shirotsuka, Hirata and Niwa, 1972). Preliminary experimental results showed that mass transfer coefficients varied unusually with both external flows in a complicated manner. Once the experimental data were rearranged according to a theoretical analysis considering the interfacial velocity, the results were well explained as shown in Fig. 1. From these results, three remarkable things can be noticed:

1. When the interfacial flow has the same direction of the bulk stream, the mass transfer rate increases with the interfacial velocity.
2. At high dimensionless interfacial velocity (ratio of the interfacial velocity to the free stream velocity), the mass transfer rate is proportional to the square root of the interfacial velocity.
3. In counter-current flow, mass transfer rate decreases against an increase in the interfacial velocity.

3.3 Momentum and mass transfer with an interfacial velocity in spherical geometries

A numerical analysis was made for the interphase momentum and mass transfer through a flowing plane interface (two-dimensional laminar boundary layer conditions, Shirotsuka et al, (1969). Approximate equations to fit the numerical solutions were obtained for both, drag and mass transfer coefficients as follows (Hirata & Suzuki, 1980):

$$\frac{C_D}{C_{DS}} = \left| 1 - \frac{u_i}{u_\infty} \right| \left[1 + (2.88 - a) \frac{u_i}{u_\infty} \right]^{1/2} \quad (1)$$

$$\frac{Sh}{Sh_S} = \left[1 + (2.88 - aSc^{-b}) Sc^{1/2} \left(\frac{u_i}{u_\infty} \right) \right]^{1/2} \quad (2)$$

where

$$a = \frac{0.09 + (u_i/u_\infty)^2}{0.10 + (u_i/u_\infty)^2}$$

$$b = \frac{3(u_i/u_\infty)}{2 + 12(u_i/u_\infty)}$$

C_{DS} and Sh_S are the values for zero interfacial velocity. They can be evaluated by the following equations for laminar boundary layer:

for a plane interface;

$$C_{DS} = 0.664Re^{-1/2} \quad (3)$$

$$Sh_S = 0.332Re^{1/2}Sc^{1/3} \quad (4)$$

for a spherical interface;

$$C_{DS} = (24/Re)(1 + 0.125Re^{0.72}) \quad (5)$$

$$Sh_S = 2 + 0.6Re^{1/2}Sc^{1/3} \quad (6)$$

Eqs. (1) and (2) with Eqs. (5) and (6) are consistently applicable to momentum and mass transfer for solid spheres, gas bubbles and liquid drops as mentioned later (Hirata, 1982, Hirata and Okano, 1984, Hirata, Nishizawa and Okano, 1992a).

From these results, three remarkable things can be noticed:

1. With increasing the dimensionless interfacial velocity, the normalized Sh number increases, while the normalized drag coefficient decreases.
2. The normalized drag coefficient is only a function of dimensionless interfacial velocity, and the normalized Sh number is a function of dimensionless interfacial velocity and Sc number. Both are independent of Re number.
3. The effect of Sc number on mass transfer changes with the interfacial velocity. Although in the case of a stationary interface, the Sh number is proportional to 1/3 power of Sc number, in the case of $Sc^{1/3}(u_i/u_\infty)$ much greater than unity, it is proportional to the square root of Sc, Re and dimensionless interfacial velocity. This means that the Sh number is proportional to the square root of $u_i x/D$. The equation is exactly the same as the Boussinesque equation.

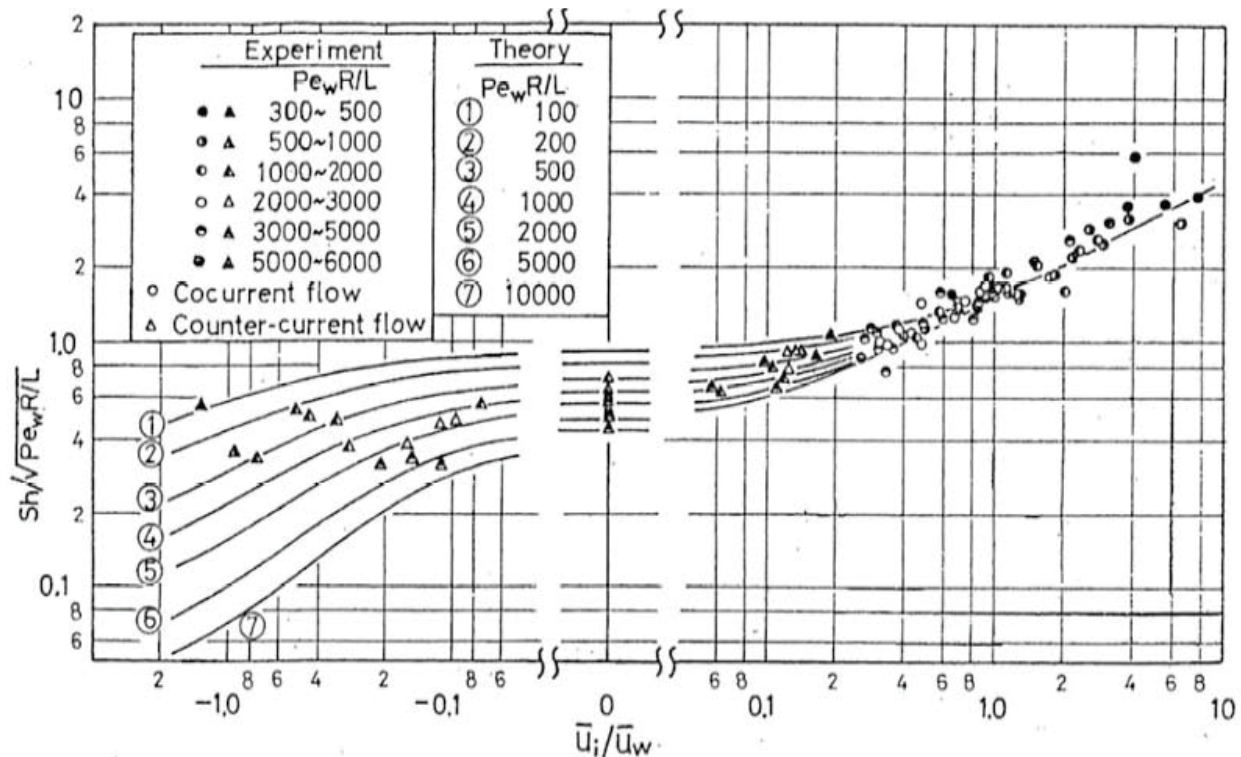


Figure 1: Mass transfer with a flowing interface separating two-laminar layers

3.4 Momentum heat and mass transfer with surface tension gradients on a planar liquid-fluid interface

When an interfacial tension gradient caused by a temperature and/or a concentration difference exists at a liquid-fluid interface, this gradient affects the interfacial velocity significantly. Consequently it also affects significantly the rates of momentum, heat and mass transfer in a complicated manner. Simple configurations of the interfacial motion affected by the interfacial tension gradient on a co-current flowing plane interface are shown in Fig. 2. In Fig. 2, case (ii) corresponds to a clean interface without any interfacial tension gradient. Case (i) is with a negative interfacial tension gradient. Case (iii) is with a positive interfacial tension gradient, where the mobility of the interface is enhanced.

The two-dimensional laminar boundary layer equations; the continuity equations, momentum equations, energy equations and diffusion equations for two different phases as shown in Fig. 2 were numerically solved with the additional inter-

facial boundary condition obtained from the continuity of tangential stress, where the interfacial tension gradient is considered (Hirata, Kawakami and Okano, 1989). A schematic diagram of typical numerical results showing the effect of the interfacial tension gradient on the interfacial velocity, the friction coefficient and the Nu number are shown in Fig. 3.

In Fig. 3, the numerical results are arranged by dimensionless groups, where the important groups are newly defined as Eqs. (7), (8) and (9).

modified friction coefficient, which should be used on the flowing interface:

$$C_{fN} \equiv \frac{\tau_s}{\rho u_\infty |u_s - u_\infty|} \tag{7}$$

$$\begin{aligned} \frac{Ma}{Re^2} &\equiv \frac{\partial \sigma / \partial x}{\rho u_\infty^2} \\ &\equiv \frac{\text{Interfacial tension gradient driven force}}{\text{Viscous force}} \end{aligned} \tag{8}$$

$$\frac{Ma}{Re} \equiv \frac{(\partial\sigma/\partial x)x}{\mu u_\infty^2}$$

$$\equiv \frac{\text{Interfacial tension gradient driven force}}{\text{Inertia force}} \quad (9)$$

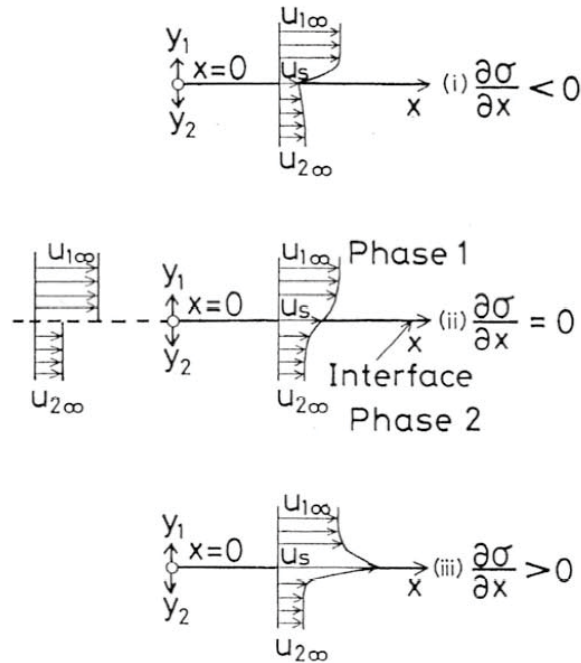


Figure 2: Interfacial motion affected by a surface tension gradient

From Fig. 3, six remarkable things can be noticed:

1. At a particular negative value of the Marangoni number, the mobility of the interface is sharply suppressed. Such a value of Marangoni number is newly defined as the negative critical Marangoni number $(Ma)_{c-}$, which is derived here theoretically as follows:

$$(Ma_1)_{c-} = -0.332Re_1^{3/2} \left[1 + \left(\frac{u_{2\infty}}{u_{1\infty}} \right)^{3/2} \left(\frac{\rho_2\mu_2}{\rho_1\mu_1} \right)^{1/2} \right] \quad (10)$$

2. Around the negative critical Marangoni number, the rates of momentum, heat and mass

transfer sharply decrease to the value at the stationary interface: $u_s = 0$, due to the suppression of the interfacial velocity.

3. Beyond a particular positive value of the Marangoni number, the interfacial velocity is gradually enhanced, and consequently the rates of momentum, heat and mass transfer are gradually increased with increase in Marangoni number. Such a Marangoni number is defined here as the positive critical Marangoni number $(Ma)_c+$ the absolute value of which is nearly equal to that of the negative critical Marangoni number.
4. When the Marangoni number is much greater than the positive critical Marangoni number, the interfacial velocity is proportional to the 2/3 power of Marangoni number, and the modified friction coefficient and the Nu number are proportional to the 1/3 power of Marangoni number.
5. In the region between the negative and positive critical Marangoni numbers, the interfacial velocity is independent of the interfacial tension gradient, consequently, the interfacial tension gradient does not affect the momentum, heat and mass transfer.
6. The interfacial contamination phenomena and the interfacial turbulence phenomena (well known to be important in liquid-liquid extraction) can be well explained, respectively, by the suppression and the enhancement of the interfacial velocity caused, respectively, by the negative and the positive interfacial tension gradient on the liquid-fluid interface.

3.5 Momentum and mass transfer through the interface of single gas bubbles and liquid drops in the presence of surface tension gradients

In order to evaluate the interfacial velocity on single gas bubbles and single liquid drops, the Navier-Stokes equations in spherical coordinates for two different phases were theoretically analyzed with the surface tension gradient considered

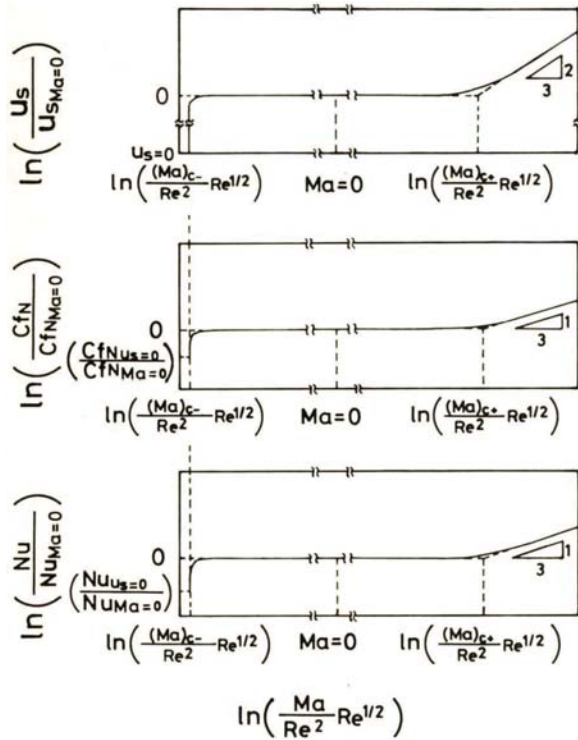


Figure 3: A schematic diagram showing the effect of surface tension gradients on the interfacial velocity, friction coefficient and Nusselt number.

as the boundary condition at the interface. The interfacial velocities were theoretically obtained in a closed form for the cases of both very low and very large Re number.

$$\frac{u_s}{u_T} = \frac{3}{8}\pi - \left[\frac{3}{8}\pi - A(1-m) \right] \exp(-DRe)I_0(DRe) \tag{11}$$

where,

$$A = \frac{1}{8(1+\kappa)}\pi$$

$$B = 2.197\sqrt{\frac{3}{\pi}} \frac{2+3\kappa+m}{1+\sqrt{\gamma\kappa}}$$

$$D = \left[\frac{3}{8}\pi - A(1-m) \right]^2 / (2\pi B^2)$$

where, m is defined as the degree of interfacial contamination as shown below:

$$m = \frac{4}{3} \left| \frac{Ma}{Re} \frac{1}{\sin\theta} \right| \tag{12}$$

When the interface is completely clean and without any surface tension gradient, m is zero. In the case of $m > 0$, the interfacial tension gradient suppresses the interfacial velocity. It is the same phenomena as the well known interfacial contamination phenomena.

The theoretical results provided by Eqs. (2) and (4) combined with Eq. (11) explain well previous experimental results for phase mass transfer from single liquid drops (Shirotsuka and Hirata, 1971a) and from single gas bubbles (Shirotsuka and Hirata, 1971b). Typical examples for comparison of the theoretical results with previous experimental results by Thorson et al (1962, 1968) for drag coefficient and Sh number in single drops are shown in Fig. 4, a) and b). It can be noticed that the experimental results for both drag coefficient and Sh number are well explained by the theoretical results for $m = 3$ (Hirata, Nishizawa and Okano, 1992a). The major outcome of Fig. 4 is that a unified (analogy) theory for momentum and mass transfer from single solid sheres, gas bubbles and liquid drops can be established.

The results calculated from the theory on the effects of γ and m on dimensionless interfacial velocity, drag coefficient and Sh number are shown in Fig. 5. From Fig. 5, the following remarks can be deduced:

1. With an increase in the values of κ and m , the interfacial velocity decreases.
2. The effect of m on the interfacial velocity at low Re number is much larger than at high Re number. This means that small drops are more sensitive to interfacial contamination than large drops.
3. The effect of m on the drag coefficient can be considered the same as the effect of κ on it. On the other hand, the effect of m on the interfacial velocity and Sh number is larger than the effect of κ .
4. The effect of m on the drag coefficient is much larger at high Re numbers than at low Re numbers. On the other hand, the effect of m on the Sh number is much lower at high Re numbers than at low Re numbers.

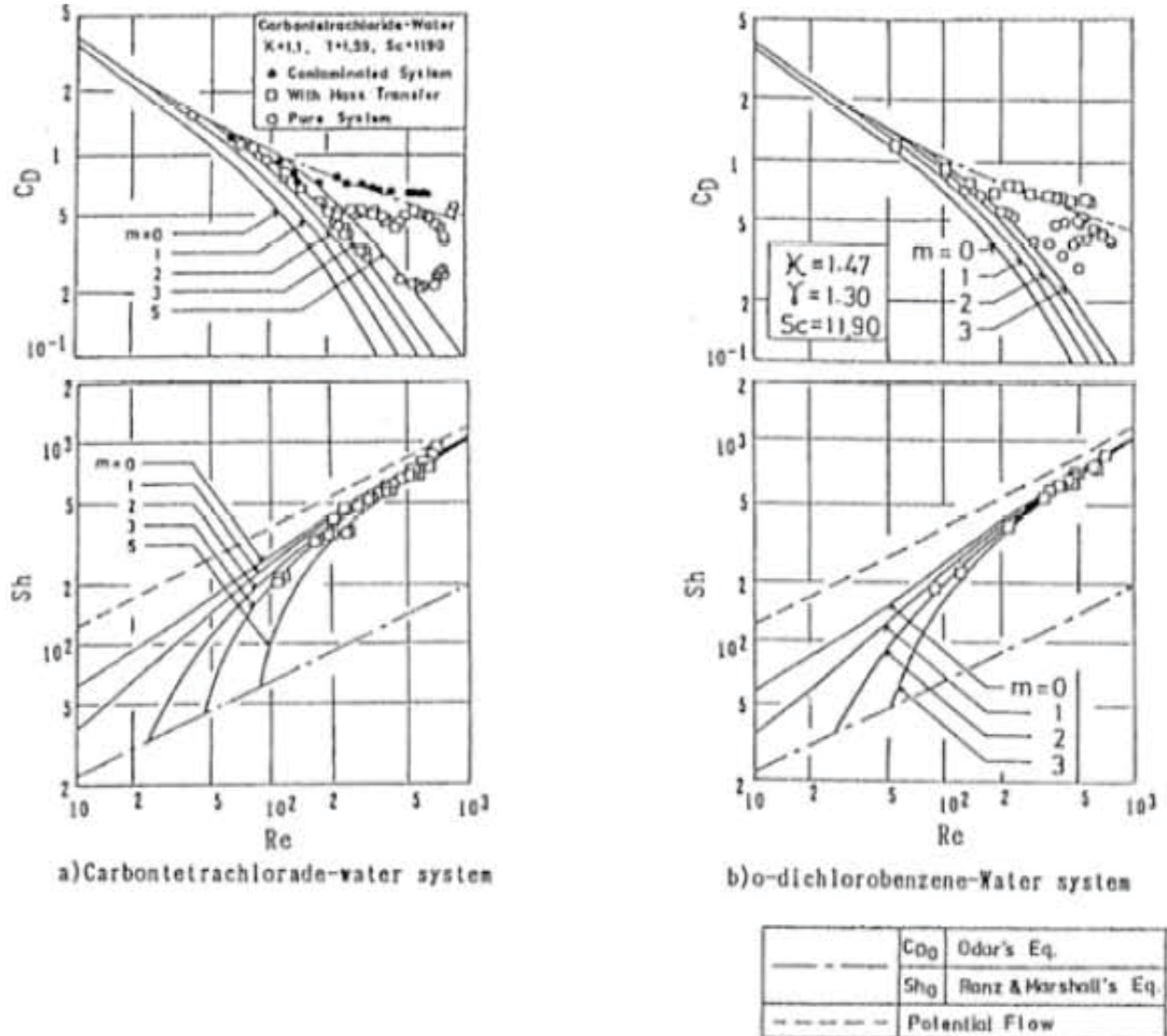


Figure 4: Comparison of theoretical results with previous experimental results

5. At particular low Re numbers, depending on the value of m , liquid drops behave like rigid spheres. The related value of m is defined as the critical contamination degree m^* .

The relationship between Re numbers and m^* is shown in Fig. 6.

From Fig. 6, the following can be deduced:

1. When $Re < 1$, the interface become rigid at $m^* = 1$.
2. When $Re \gg 1$, the following relationships are

obtained:

$$m^* \propto Re^{1/2} \tag{13}$$

$$Ma_{c-} \propto Re^{3/2} \tag{14}$$

The negative critical Ma number, Ma_{c-} at which liquid drops behave like rigid spheres is proportional to $3/2$ power of the Reynolds number, the same as in Eq.(10) mentioned earlier.

3. With an increase in the value of κ , the negative critical Ma number increases.

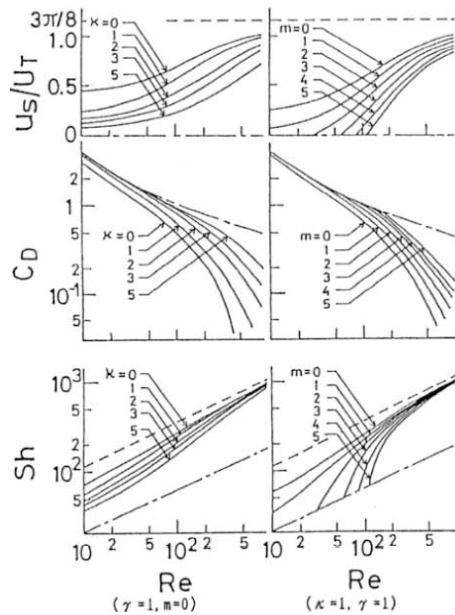


Figure 5: Effects of κ and m on interfacial velocity, drag coefficient and Sherwood number ($Sc=1000$)

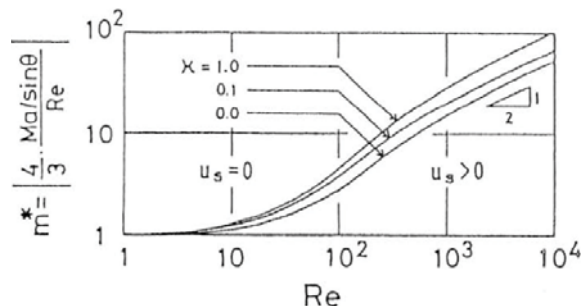


Figure 6: Relationship between Reynolds number and m^* , the critical value of m for which the interface behaves as a rigid surface ($\gamma=1$)

4 Transport phenomena in single crystal growth from melt

Since single crystal growth is a process coupled in a complicated manner with momentum, heat and mass transfer, as well as phase transition and chemical reaction, the quality of single crystals is significantly influenced by convection.

In bulk single crystal growth from melt by the Bridgman method, the floating zone method and Czochralsky (CZ) method, works as late as the 1980's had only considered forced and natural

convection. The author has made clear the inter-phase transport phenomena on crystal-melt interface and melt-ambient gas interface with surface tension gradients driven convection (Marangoni convection) taken into account. From these works, important knowledge for the high quality production of bulk single crystals from melt has been obtained.

4.1 Transport phenomena in Bridgman method

4.1.1 Solidification problem

The author developed a numerical method for solving the two-dimensional unsteady one-directional solidification problems by using a boundary-fitted co-ordinate system (Saitou and Hirata, 1991a, 1991b, 1993), and proposed the optimal operational conditions for high quality crystals (Saitou and Hirata, 1992c). Important information was provided about the solid-liquid interface shape (Saitou and Hirata, 1991c, 1992a), the ratio of liquid to solid thermal conductivity (Saitou and Hirata, 1992b) as well as the interfacial stability, which significantly influence the quality of single crystals.

4.1.2 Thermal and solutal natural and Marangoni convection

Natural and Marangoni convection formed spontaneously in a melt inside a two-dimensional rectangular open boat were investigated by means of an order-of-magnitude evaluation and numerical analysis (by the finite difference method). A quantitative evaluation was made of the Gr number, Ma number, Pr number and melt depth, all of which affect the interfacial velocity and the velocity distribution of the melt convection. It was concluded that Marangoni convection is important when the melt is shallow (Okano, Itoh and Hirata, 1989a). Interfacial velocities induced by solutal Marangoni convection were also measured in In-Ga-Sb systems (initial bulk melt with an additional material contacting the bulk interface, Arafune and Hirata, 1999a). Empirical and theoretical correlation for Re numbers based on maximum interfacial velocities induced by the Marangoni convection was obtained as follows

over a wide range of Pr numbers (Arafune, Sug-iura and Hirata, 1999b):

$$\text{Re} \geq 1; \quad \text{Re} = 0.28 \left(\text{Ma} \text{Pr}^{-1/2} \right)^{2/3} \quad (15)$$

$$\text{Re} \leq 1; \quad \text{Re} = 0.049 \text{As}^{1/2} \text{Ma} \quad (16)$$

4.1.3 Magnetic field effects

The effects of magnetic fields on Marangoni and natural convection were studied numerically. Convective velocities in magnetic fields depend on the Ma number, Gr number, as well as the physical properties, and the direction and strength of the applied magnetic field. For suppression of natural convection, both horizontal and vertical magnetic fields are effective. The suppression of Marangoni convection is more difficult than natural convection, and a vertical magnetic field is more effective than a horizontal one. The interfacial velocity induced by natural convection is inversely proportional to the Hartmann number. That induced by Marangoni convection is inversely proportional to the square root of the Ha number (Hirata, Tachibana, Okano and Fukuda, 1992b).

4.1.4 Coupled thermal and solutal Marangoni convection

Experimental and numerical studies were performed on thermal and solutal Marangoni convection occurring during the growth of InSb from melt of $\text{In}_{1-x}\text{Sb}_x$.

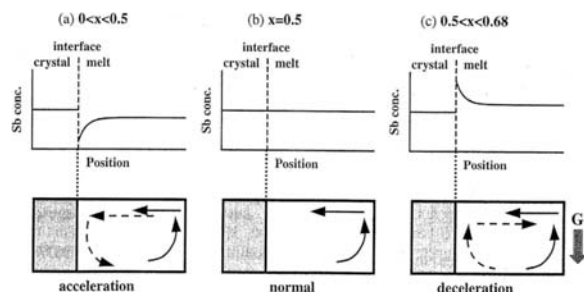


Figure 7: Schematic concentration distribution (upper) and flow direction (lower): solid-line and dashed-line arrows in lower illustration indicate, respectively, thermal and solutal convection

Fig. 7 shows the schematic diagram of the concentration distribution of Sb and the interfacial flow direction for three typical cases:

1. Case (a): Acceleration.
When $0 < x < 0.5$, the interfacial flow is more accelerated than in the normal case (b), because thermal and solutal flows have the same direction.
2. Case (b): Normal.
When $x = 0.5$, it is a normal case, where only thermal Marangoni convection exists inside the melt.
3. Case (c): Deceleration.
When $0.5 < x < 0.68$, the interfacial flow is decelerated with respect to case (b), because thermal and solutal effects counteract.

Fig. 8 shows that the above considerations explain the experimental results well. It can be demonstrated from Fig. 8 that the solutal Marangoni convection is more important than the thermal one in the growth of single crystals of semiconductors and chemical compound semiconductors (Arafune and Hirata, 1998, 1999a, Arafune, Yamamoto and Hirata, 2001).

4.1.5 Crystal-melt interface shape control

It is worth noting that the solutal Marangoni convection has been experimentally considered as a new important control parameter in addition to convectional control parameters such as the temperature gradient and cooling rate in order to obtain a planar crystal-melt interface in InSb crystal growth. It can be concluded from the experimental results that the utilization of solutal Marangoni convection can effectively allow the control of the crystal-melt interface shape without changing the temperature gradient or the cooling rate (Arafune, Kodera, Kinoshita and Hirata, 2003).

4.2 Transport phenomena in floating zone (FZ) method

Natural and Marangoni flows produced in a melt during single crystal growth by the floating zone method were analyzed by an order-of-magnitude

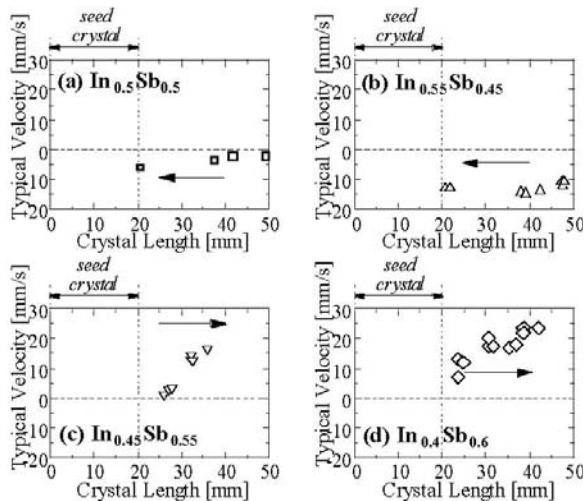


Figure 8: Relation between crystal length and typical interfacial velocity. Arrows show the flow direction near the interface; x_{init} = (a) 0.5, (b) 0.45, (c) 0.55, (d) 0.6

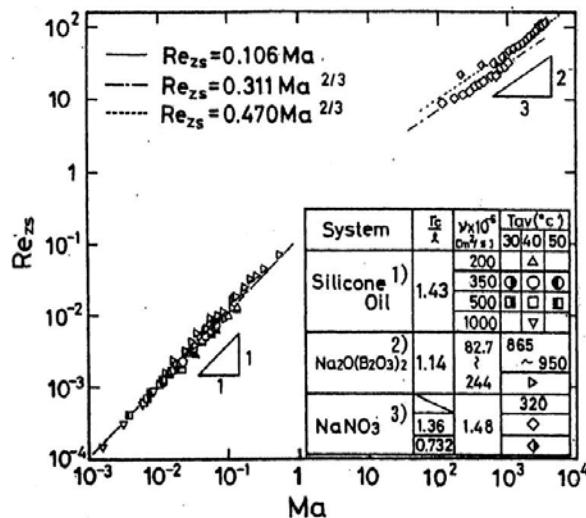


Figure 9: Comparison of analytical results shown in Table 1 with previous experimental results. 1) McNeil et al.(1984), 2) McNeil et al. (1985), 3) Preisser et al.(1983)

evaluation (Okano, Hatano and Hirata, 1989a, Hirata, Nishizawa, Imaishi, Okano, Saghir and Scott, 1991). The analytical results on the effects of Marangoni and natural convections on Re numbers based on free interfacial velocity are shown in Table 1. Comparison of the analytical results with previous experimental results is shown in

Fig. 9. It can be seen from Fig. 9 that the analytical results are in good agreement with previous experimental results for the case of Marangoni convection in a vertical capillary liquid bridge (model liquids and glass melt).

These results have been effectively applied to elucidate the mechanism of Marangoni convection phenomena under microgravity conditions as mentioned later.

4.3 Transport phenomena in Czochralski(CZ) method

The crystal-melt interface shape is one of the important variables in determining the quality of bulk single crystals.

It is significantly influenced by convection in melt. In order to obtain high quality uniform single crystals, it is necessary that the interfacial shape should be kept in a plane (Hirata et al., 1992c). Although previous research had only considered forced convection due to crystal and crucible rotations, and natural convection due to temperature distribution in melt, the author considered Marangoni convection in addition to the forced and natural convections, and proposed an evaluation method for determining which convection is dominant in melt, as shown in Fig. 10 (Okano, Tachibana, Hatano and Hirata, 1989c, Hirata et al., 1992a) for the case of boundary layer flow regime as a typical example. Once experimental results for the critical rotation rate ω^* , at which a plane interface shape is obtained at the crystal rotation rate, are arranged based on Fig. 10, it can be seen that when the value of ordinate is constant, the natural convection is dominant in melt, and when the value of ordinate is proportional to the value of abscissa, the Marangoni convection is dominant. The previous experimental results have been rearranged based on Fig. 10, and are shown in Fig. 11, where only controllable variables in the dimensionless groups in Fig. 10 are used. Fig. 12 shows an example of comparison of previous experimental results during growth of Gd₃Ga₅O₁₂ (GGG) with theoretical results in the case of Marangoni convection dominant condition (Fig. 12(a)) and in the case of natural convection dominant condition (Fig. 12(b)).

Table 1: Analytical results on natural and Marangoni convections in a floating zone

| | Re \ll 1 | | Re \gg 1 | |
|--------------------------------------|-----------------------|---------------------------------|--|----------|
| | Pr \leq 1, Pr $>$ 1 | Pr $<$ 1 | Pr $<$ 1 | Pr $>$ 1 |
| Natural convection dominant regime | $\frac{Ma}{Gr} < 1$ | $\frac{Ma^{2/3}}{Gr^{1/2}} < 1$ | $\frac{Ma^{2/3}}{Gr^{1/2}} Pr^{1/6} < 1$ | |
| | Re \propto Gr | Re \propto Gr $^{1/2}$ | Re \propto $\frac{Gr^{1/2}}{Pr^{1/2}}$ | |
| Marangoni convection dominant regime | $\frac{Ma}{Gr} > 1$ | $\frac{Ma^{2/3}}{Gr^{1/2}} > 1$ | $\frac{Ma^{2/3}}{Gr^{1/2}} Pr^{1/6} > 1$ | |
| | Re \propto Ma | Re \propto Ma $^{2/3}$ | Re \propto $\frac{Ma^{2/3}}{Pr^{1/2}}$ | |

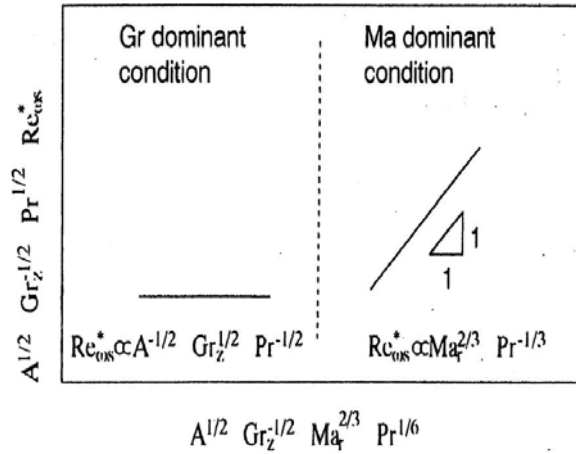


Figure 10: Diagram for determining the dominant convection in the melt—The case of boundary layer flow regime

It can be pointed out from Figs. 11 and 12 that the Marangoni convection is very important and dominant in the melt in most of these experiments, and should be considered in order to control the crystal-melt interface shape. The theoretical and empirical relation between the critical crystal rotation and operational conditions is proposed as follows (Okano et al., 1989c, 1991, Hirata et al., 1993a, 1993b, Tachibana et al., 1990):

$$\omega^* \propto \left(\frac{\Delta T}{\Delta r}\right)^{2/3} \left(\frac{\Delta r}{r_c}\right)^{1/3} \quad (17)$$

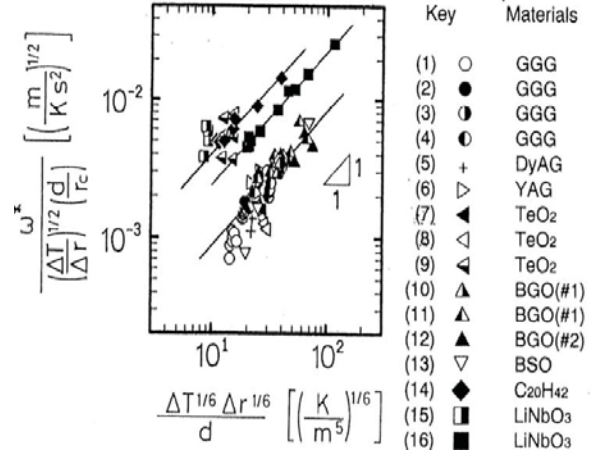


Figure 11: Evaluation of the dominant convection conditions in terms of dimensionless numbers (1), (2) Miller et al. (1978); (3), (4) Takagi et al. (1976); (5) Miyazawa et al. (1978); (6) Miyazawa et al. (1978); (7) Miyazawa and Kondo (1973); (8) Miyazawa (1980); (9) Lukasiewicz et al. (1992); (10) Berkowski et al. (1987); (11), (12) Berkowski et al. (1991); (13) Brice et al. (1974); (14) Hirata et al. (1993a); (15) Trauth and Grabmaier (1991); (16) Hirata et al.(1993b).

4.4 Chemical compound semiconductor by Laser-MOVPE

4.4.1 Atomic monolayer epitaxy of chemical compound semiconductor by Laser-MOVPE

A new technique for obtaining atomic monolayers of semiconductors via vapor phase epitaxy from metal organic compounds exposed by laser beam (to prepare three dimensional super lattice LSI) was developed by Meguro et al., (1988, 1990a) for

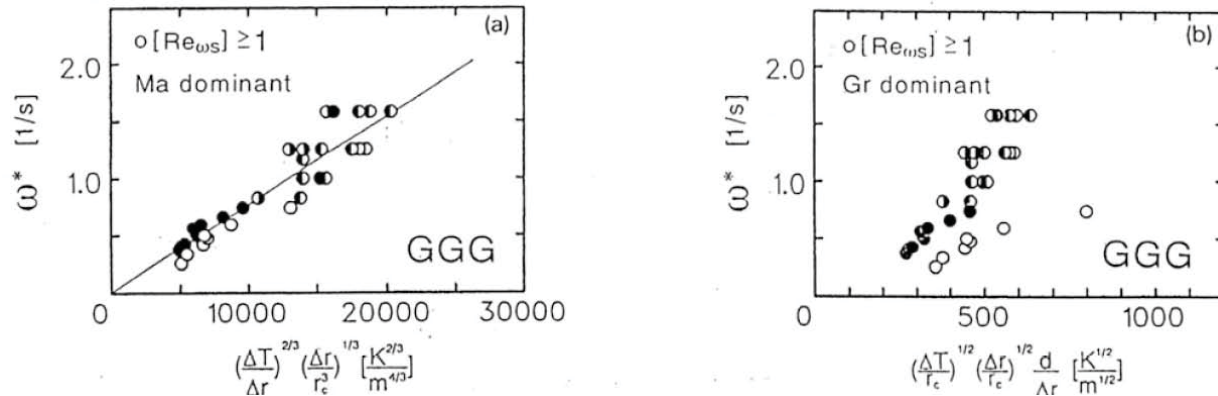


Figure 12: Comparison of theoretical results with previous experimental results (GGG) (a) dominant Marangoni convection (b) dominant natural convection

GaAs, and Meguro et al., (1990b) for AlAs and GaAlAs. Self-limiting Ga deposition on GaAs during laser-atomic epitaxial processing was directly observed and the related mechanism was elucidated by Simko et al. (1992).

4.4.2 Room temperature UV-emission at 345nm from InAlGaN-based light-emitting diodes

Optical and electrical properties of 340 nm-band bright UV-light emitting diodes (LEDs) were compared among $\text{In}_{0.03}\text{Al}_{0.20}\text{Ga}_{0.77}\text{N}$ and other active regions (Hirayama et al., 2000a, 2000b, 2001a, 2001b, Kinoshita et al., 2000a, 2000b, 2000c). Single peaked and high efficiency ultraviolet (UV) emission at 345 nm from $\text{In}_{0.03}\text{Al}_{0.20}\text{Ga}_{0.77}\text{N}$ LEDs were achieved under continuous current injection conditions (Kinoshita et al., 2001a). Significant broadening and peak shift of the electroluminescence (EL) spectrum were not observed. Such a good behavior can be attributed to the high quality InAlGaN-quaternary active layer (Hirayama et al., 2001b). The EL intensity of the InAlGaN quaternary-based LED showed more than one order of magnitude higher intensity than that of AlGaN and GaN based LEDs. Additionally, InAlGaN quaternary-based LEDs show a linear increase in intensity with increasing injection current from the I-L characteristics, that is also observed for InGaN based LEDs (Hirayama et al., 2001b). This shows that the recombination efficiency of the InAlGaN-based LEDs is as high as that of InGaN based

LEDs. From these results InAlGaN quaternary is expected to be a promising material for UV LEDs and LDs (Hirayama et al., 2002).

5 Transport phenomena under microgravity conditions

As already explained before, when single crystals are grown from a melt, the quality of the single crystals is seriously affected by convection induced by temperature and concentration differences in the melt. Therefore, thermocapillary Marangoni convection induced by a temperature difference on melt interface, and solutal Marangoni convection induced by a concentration difference on melt interface, are very important for the quality of single crystals under μg conditions. The author has elucidated the mechanism of thermocapillary and solutal Marangoni flows under μg conditions via drop shafts, parabolic flights, sounding rocket, space shuttle and recoverable satellite as well as on the ground.

5.1 Development of equipments and operations for microgravity experiments

Novel equipments and operations are necessary for μg experiments significantly differing from for ground ones. A facility is required to be compact and able to do experiments automatically in very short time, for instance, within 5 seconds in case of a drop shaft experiment. The author developed novel experimental equipments to get a stable formation of a liquid bridge even with a se-

rious change of gravity in a drop shaft, parabolic flight or sounding rocket experiment (Azuma et al., 1990, Yoshitomi et al., 1992).

Also a three-dimensional in-situ observation technique to measure velocity and temperature distributions was developed (Yoshitomi et al., 1992; Hirata et al., 1993c, 1994, 1997a).

5.2 Interfacial contamination in a silicone oil liquid bridge

Silicone oils are widely used as model fluids to study convection phenomena inside the Floating Zone, because silicone oil is transparent and its physical properties are well known. Through many experimental studies it has been found for methyl-phenyl silicone oil (KF-56) that interfacial contamination is caused by water slightly included in the silicone oil itself and also by water vapor in the surrounding atmosphere (Hirata et al., 1993d, 1993e). Since interfacial contamination leads to a significant decrease in the interfacial velocity and weakens Marangoni convection, it should be pointed out that much attention should be paid to complete dehydration of both silicone oil and the surrounding gas.

5.3 Laminar thermocapillary convection in a liquid bridge during parabolic flight

Laminar thermocapillary Marangoni convection in a liquid bridge with silicone oils (KF-96: 5, 10, 20, 50 cSt and KF-56: 15 cSt) was observed under μg conditions during a parabolic flight (Hirata et al., 1994). Fig. 13 shows that the relationship between Ma numbers and Re numbers based on the interfacial velocity caused by thermocapillary Marangoni convection, at the center of the free interface of the liquid bridge. It can be seen that the experimental results are in good agreement with the previous theoretical results shown in Table 1 (Okano et al., 1989b). In the aforementioned works, Axis-symmetric laminar Marangoni convection was studied experimentally and numerically.

The initial temperature conditions inside a liquid bridge, heat transfer across the free interface, and temperature dependence on both velocity and temperature field were also made clear.

| L [mm] | KF96 | | | | KF56 |
|-----------|------|-------|-------|-------|-------|
| | 5cSt | 10cSt | 20cSt | 50cSt | 15cSt |
| 5 | ▲ | | ▼ | ■ | ● |
| 10 | △ | ◇ | ▽ | □ | ○ |
| 15 | | ◆ | ▼ | | ● |

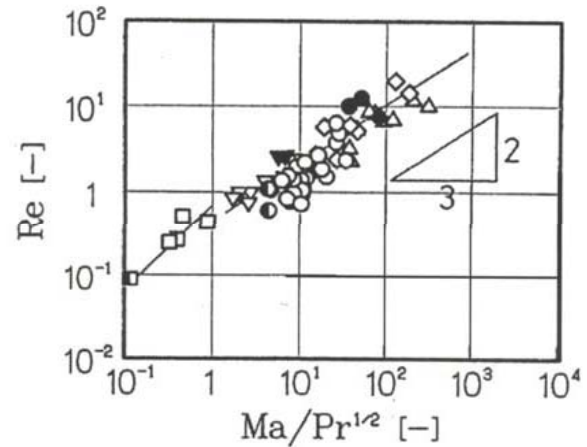


Figure 13: Relationship between Marangoni numbers and Reynolds numbers based on the interfacial velocity

5.4 Oscillatory thermocapillary convection in a liquid bridge with TR-1A sounding rocket

Laminar and oscillatory three-dimensional thermocapillary Marangoni convection in a liquid bridge of a silicone oil: 6 cSt (mixed with 20vol% of KF96L:1cSt and 80vol% of KF56:15cSt) was observed during 6 minutes μg condition with TR-1A sounding rocket No. 2 in August, 1992 (Hirata et al., 1993c)

There were two stages for the experimental sequence: at the first stage, the temperature difference between the ends of the liquid bridge was small, 30°C between 90 and 215 second, and at the second stage, the temperature difference was increased up to 50°C between 330 and 441 second.

Laminar thermocapillary Marangoni convection was observed at the first stage and oscillatory thermocapillary Marangoni convection was observed in the second stage. The experimental results on the interfacial velocity caused by the laminar Marangoni convection were explained according

to previous results (Hirata et al., 1989) and numerical analyses (Hirata et al., 1991a, 1993c). The time history of the interfacial velocity at the center of free interface caused by oscillatory Marangoni convection is shown in Fig. 14. The Fourier spectrum for temperature oscillation inside the liquid bridge between 360 and 440 second is shown in Fig. 15. The amplitude of both velocity and temperature fluctuation increased with time elapsed. The main frequency of the temperature oscillations was 0.097Hz as shown in Fig. 15 which was the same as that of the velocity field oscillation.

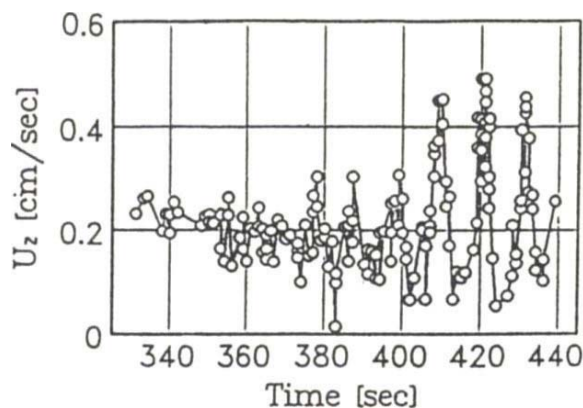


Figure 14: Interfacial velocity in a liquid bridge (TR-1A sounding rocket experiment)

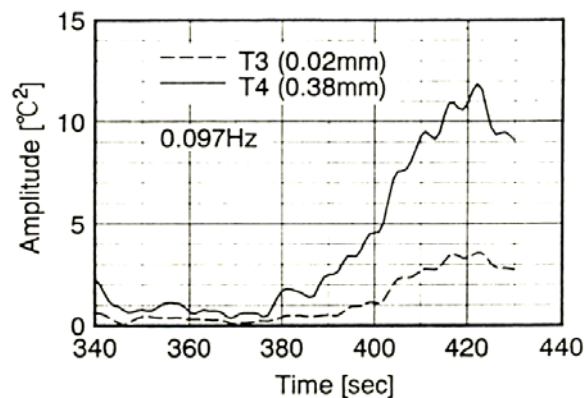


Figure 15: Fourier spectrum ($\nu=6\text{cst}$, $D=15\text{mm}$, $L=10\text{mm}$ TR-1A sounding rocket experiment)

5.5 Gravity effects on oscillatory features of thermocapillary convection in liquid bridges

Oscillatory thermocapillary Marangoni convection in silicone oil liquid bridges was observed under both normal gravity (1g) condition (Hirata et al., 1997b) and μg condition with the drop shaft facility of JAMIC (Yao et al., 1997, Hirata et al., 1997c). Examples of the typical oscillatory temperature distribution under 1g condition are shown in Photo 1, where thermal sensitive liquid crystals used there change their color from red (37.5°C) to green (40°C) and blue (42.5°C). In the horizontal view, the cold region, which is colored red, moved around the center of the liquid bridge in a counter clockwise movement. In the vertical view, non-axisymmetrical flows were observed. As the temperature difference between disks increased, both amplitude and frequency of temperature fluctuations increased.

Under the same temperature differences, as the length of a liquid bridge increased, the amplitude also increased, but the frequency decreased.

It was found that the fundamental frequency of temperature oscillations as well as the critical temperature difference (at which laminar convection changes to oscillatory one under μg conditions) were different with respect to 1g conditions, and strongly dependent on the ratio of the liquid bridge volume to the volume of a cylinder with the same radius and height (Hirata et al., 1997c). For instance, the fundamental frequency of temperature oscillations under μg conditions was smaller than under 1g conditions when the non-dimensional liquid bridge volume was $V/V_0=73.8$ vol%, (when $V/V_0=88.1$ vol%, however, it was larger under μg conditions than under 1g conditions).

5.6 Transition process from laminar to oscillatory thermocapillary convection in liquid bridges under gravity (1g) and microgravity (μg) conditions

The critical temperature difference and the temperature oscillatory features were carefully observed under 1g and μg conditions by drop shaft

with close attention paid to the liquid bridge volume (Hirata et al., 1997d, Sakurai et al., 1999).

Typical examples of the temperature signals and FFT under 1g and μg conditions are shown in Fig. 16 where the symbols are related to the temperature signal state as follows:

- (S): laminar steady state
- (P): periodic oscillatory state
- (QP): quasi periodic oscillatory state
- (C): chaotic state
- (P2): period doubling oscillatory state
- (QP+P2): mixture of (QP) and (P2)

As shown in Fig. 16, the temperature at the cool bottom of the liquid bridge under μg conditions was higher than under 1g, except for the longest liquid bridge ($L=3.3\text{mm}$) for which (P) under 1g conditions was replaced by (S) for μg .

The temperature signals can be classified into 6 patterns when the gravity changes from 1g to μg as follows:

- for drop shaft experiments: a-i): (S) \rightarrow (P)
- a-ii): (P) \rightarrow (P)
- a-iii): (QP) \rightarrow (P)
- a-iv): (C) \rightarrow (P)
- for ground experiments: b-i) (P2)
- b-ii) (QP+P2)

Fig. 17 shows the temperature signal states diagram for V/V_0 vs. ΔT , where the plus sign + shows the transition point between (S) and (P) and the cross sign \times shows the transition between (S) and (P).

From Fig. 17, five remarkable things can be noticed:

1. The critical temperature difference is very sensitive to the liquid bridge volume.
2. Under 1g conditions, the temperature signals show the existence of six states as shown in Fig. 17, but under μg conditions, all temperature signals shows only two states: (S) and (P).

3. The shorter the liquid bridge length is, the higher the critical temperature difference is, under both 1g and μg conditions.
4. For the liquid bridge with length $L=1.6$ mm, a very high critical temperature difference is observed between 70 and 80 vol% of liquid volume under 1g conditions, while under μg conditions, the critical temperature difference is remarkably lower. It means that there are some ranges of the liquid bridge volume ratio where the regime is (S) under 1g conditions but (P) under μg conditions (cf. Fig. 17 a-i) and b-i)).
5. For the liquid bridge with length $L=3.3$ mm, there are some ranges of the liquid bridge volume ratio where the convection is (P) under 1g conditions, but (S) under μg conditions.

5.7 Flow structure of time-dependent thermo-capillary convection in liquid bridges

The flow structure of time-dependent three-dimensional thermal Marangoni convection in silicone oil liquid bridges was further observed in the horizontal section by Arafune et al. (2000) and Kinoshita et al. (2001b). It was found that there was a polygon-shaped stagnant region around the central axis of a liquid bridge, and the periodic oscillatory state (P) could be further classified into periodically pulsating (Ps) and periodically rotating (P_T) states.

Figure 18 shows schematic motions of the stagnant region in the horizontal section for (Ps) and (P_T). It can be seen in Fig. 18 that (Ps) exhibits a coherent phase with a different amplitude depending on the azimuthal angle and (P_T) shows a phase shift for each azimuthal angle with same amplitude, while (QP) shows the mixture of these two types of temperature fluctuations. With increasing the temperature difference, the temperature and velocity fields exhibit the following states: (S) – (Ps) – (QP) – (P_T). This transition process depends on the liquid bridge volume and gravity level, but occurs for all kinematic viscosities and liquid bridge lengths considered.

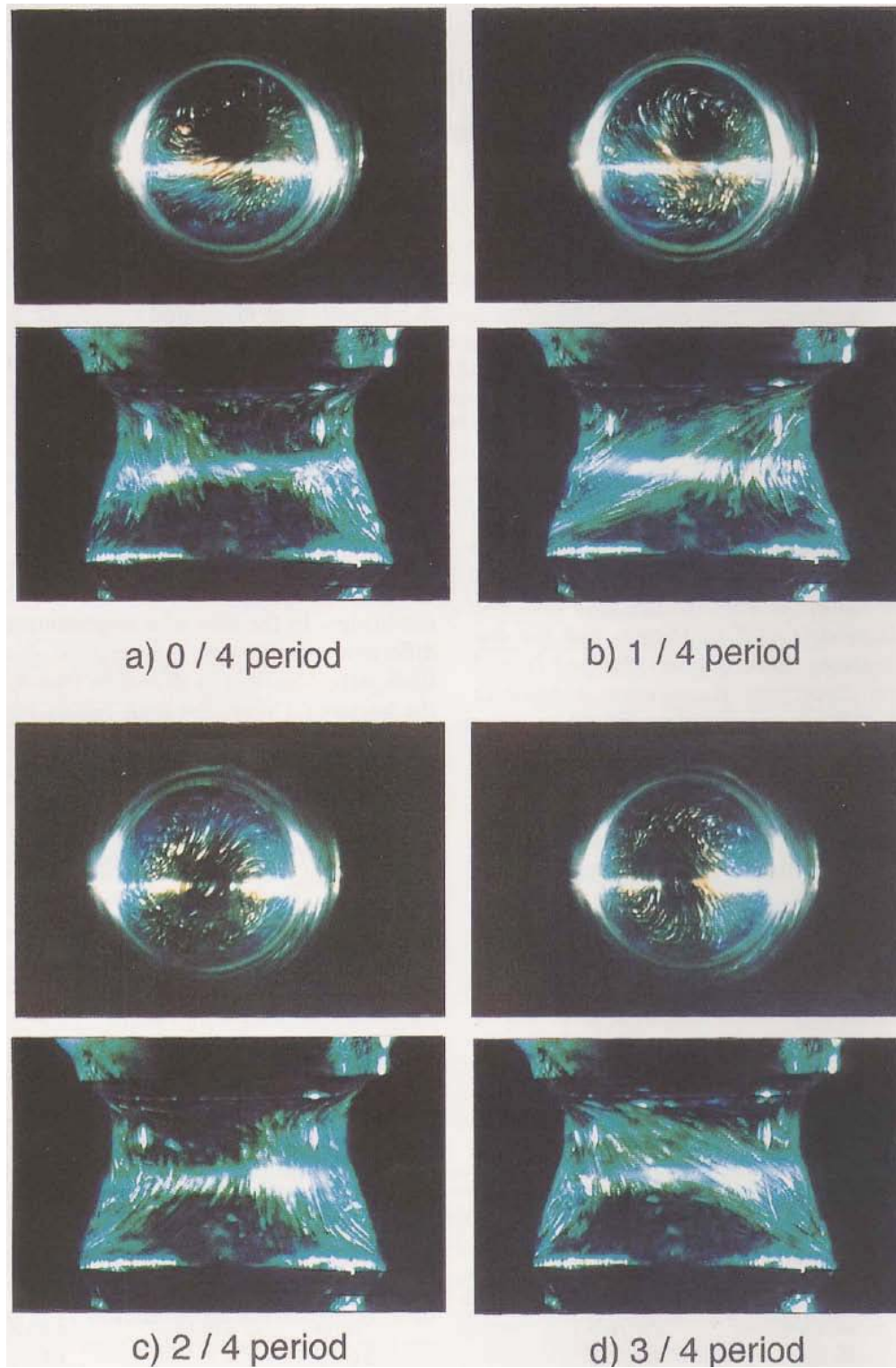


Photo 1: Observation of oscillatory Marangoni convection ($D=5\text{mm}$, $L=3.0\text{mm}$, $V/V_0=67\text{vol}\%$, $\nu=2.3\text{cSt}$, $\Delta T=27.5^\circ\text{C}$).

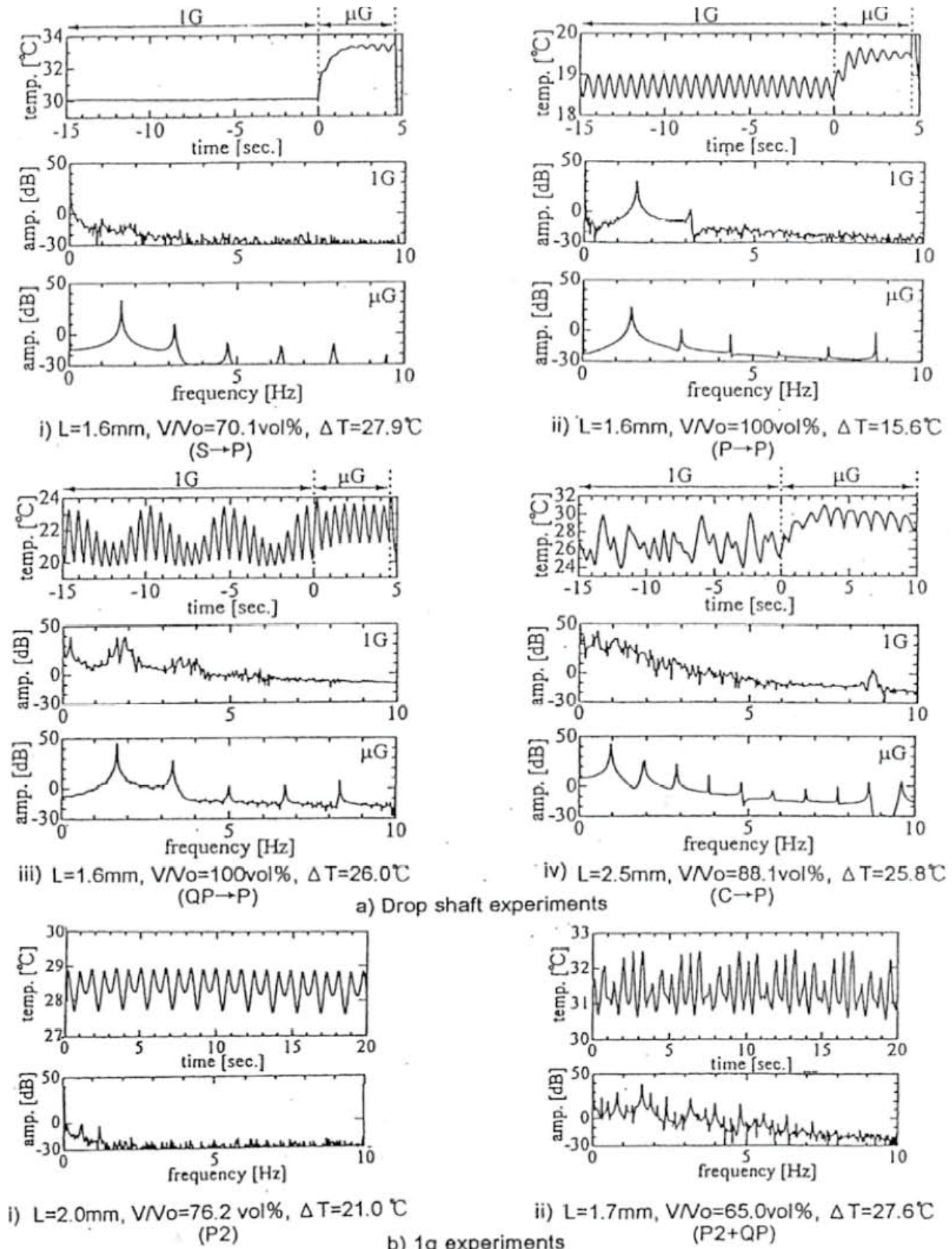
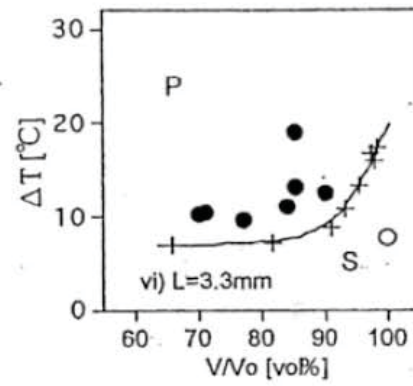
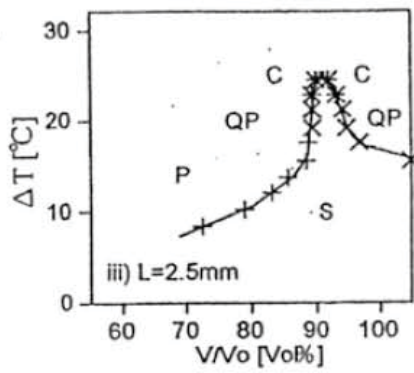
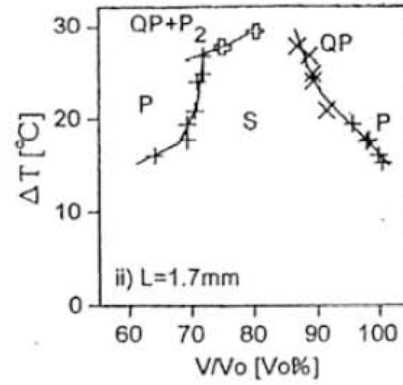
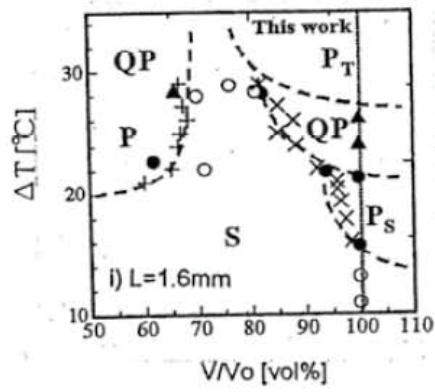
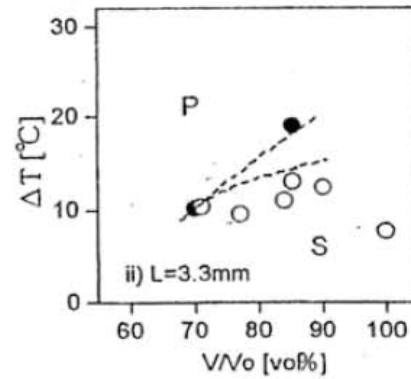
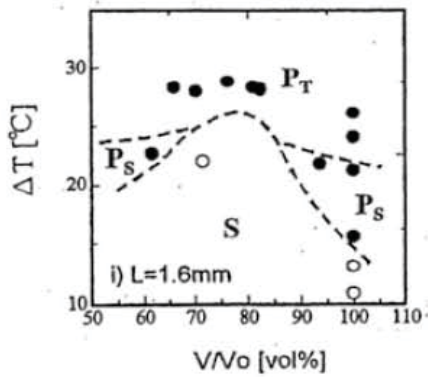


Figure 16: Typical temperature signals and FFT spectra ($D=5\text{mm}$, $v=2cSt$)



a) 1g condition



b) μg condition

Figure 17: Diagram of temperature signal states in the $V/V_0 - \Delta T$

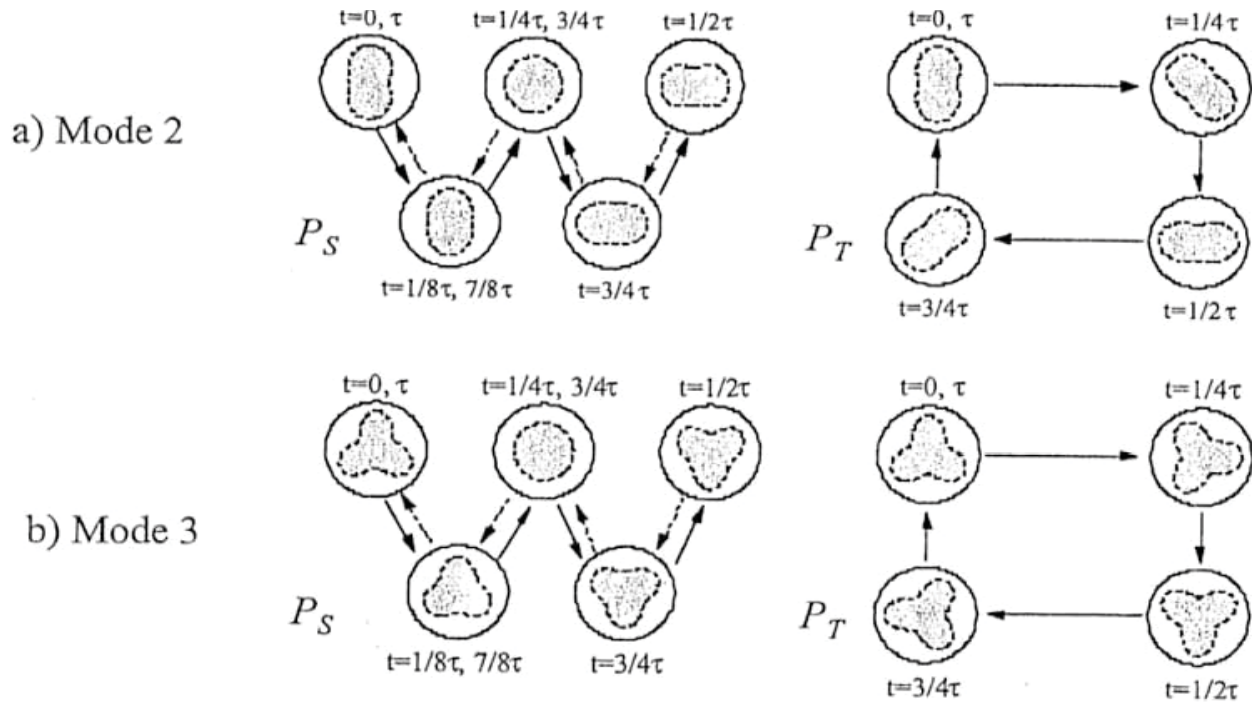


Figure 18: Schematics of the typical flow structure for pulsating (P_S) and rotating (P_T) phases with wavenumber $m = 2$ (a) and $m = 3$ (b).

5.8 Uniform mixing of melt of multi-component chemical compound semiconductors by solutal Marangoni convection: Space Shuttle experiment on IML-2 Mission

A microgravity experiment on “Uniform mixing of Melt of Multicomponent Chemical compound Semiconductor”, was carried out aboard Space Shuttle mission in July 1994 (Hirata et al., 1996, Okitsu et al., 1996, 1997). Six samples shown in Fig. 19 which were composed of In-Sb (M-1, D-1) and In-GaSb-Sb (M-1,-2, -3, -3', D-2) were melted by a uniform temperature furnace and cooled down rapidly to be solidified. M-samples and D-samples were mixed, respectively, by solutal Marangoni convection due to concentration gradient at the melt-air interface, and by molecular diffusion only. The concentration distributions of In, Ga and Sb in axial direction for D-2, M-2, -3, -3' samples composed of In-GaSb-Sb are shown in Fig. 20. It can be noticed from Fig. 20 that M-samples are more uniform than D-sample.

It has been also noticed from the comparison

of μg -samples with 1g-samples (Okitsu et al., 1994) that μg -samples show more uniform concentration distribution than 1g-samples, because the gravity convection and segregation can be suppressed under μg conditions. Numerical simulations also justify the quick mixing by the solutal Marangoni convection (Yasuhiro et al., 1997).

5.9 Dissolution and recrystallization processes of chemical compound semiconductors with the Chinese recoverable satellite and parabolic flights

The effects of gravity and crystal orientation on the dissolution of GaSb into melt and the recrystallization of InGaSb were investigated under 1g and μg conditions with a Chinese recoverable satellite (Hayakawa et al., 2000) and airplanes (Hayakawa et al., 2001, 2002). Numerical simulations were also carried out for the effects of gravity on the solid-melt interface and compositional profiles (Ozawa et al., 2000, 2001, Hayakawa et al., 2000, 2002, Okano et al., 2002, 2003). The InSb crystal was melted and GaSb was dissolved partially into the InSb melt, and then formed In-

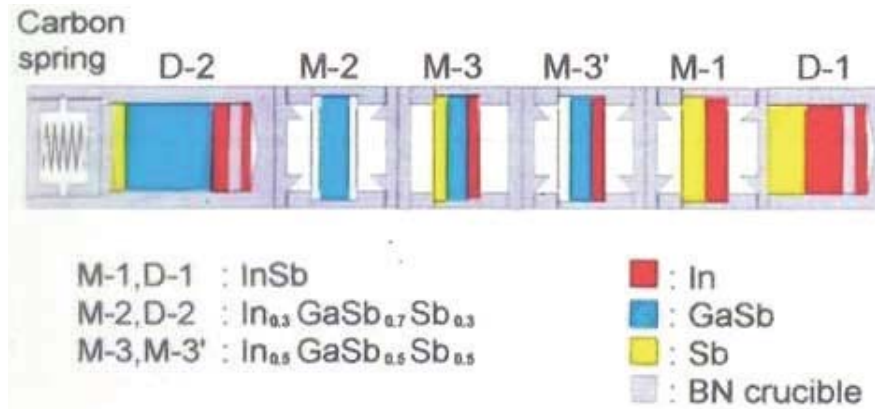


Figure 19: Configuration of samples for the Space Shuttle experiment

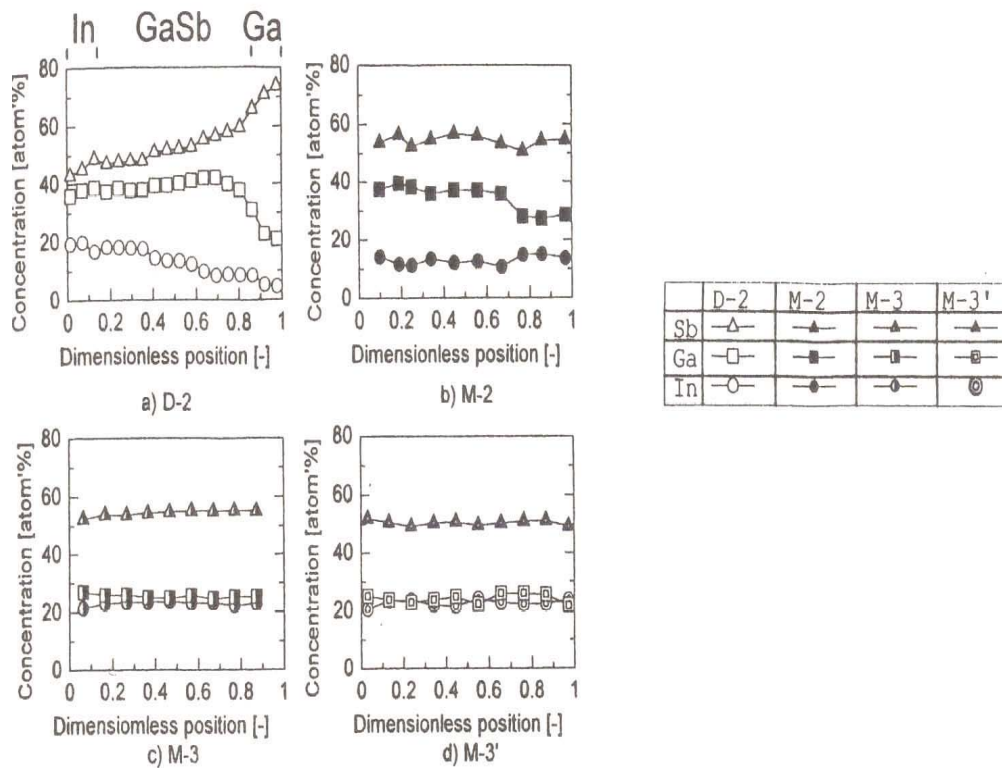


Figure 20: Concentration distribution of In, Ga and Sb in axial direction for μg samples D-2, M2, M-3 and M3'

GaSb solution which was solidified during cooling process. The experimental and numerical results clearly show that the shape of the solid-melt interface and compositional profiles in the solution were significantly affected by the gravity level (Fig. 21). It can be seen from Fig. 21 that under μg conditions, the Ga compositional profiles are uniform in the radial direction, the interfaces are almost parallel, and on the contrary, un-

der 1g conditions, as large amounts of Ga moved up to the upper region due to buoyancy, the dissolved zone broadens towards gravitational direction.

During the cooling process, needle crystals of InGaSb started appearing and the value of x in $\text{In}_x\text{Ga}_{1-x}\text{Sb}$ crystals increased with a decrease in temperature. The GaSb with the (111)B plane dissolved into the InSb melt much more than that

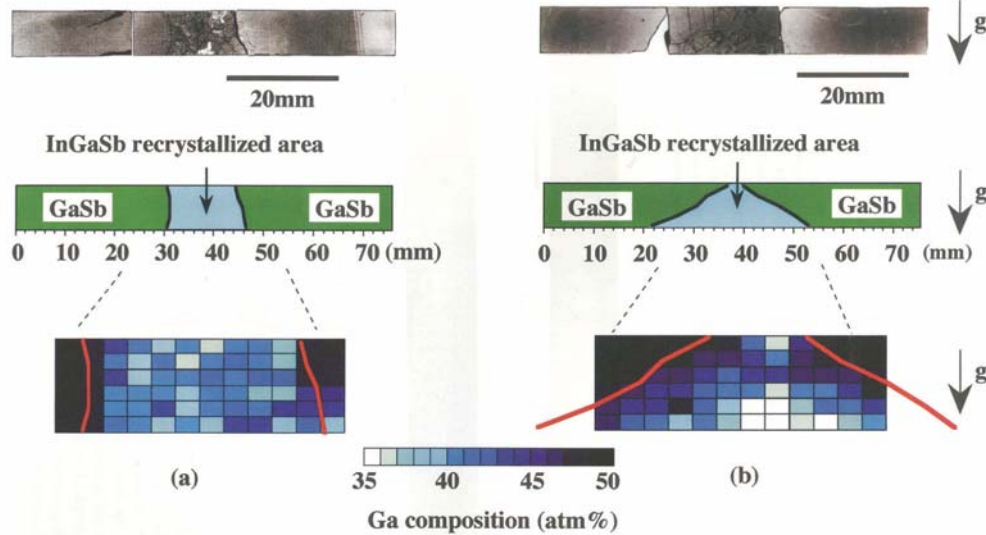


Figure 21: Morphology of the cut surface, schematic representation of the dissolved area, and Ga compositional profile around the center of the (a) space sample, (b) earth sample. The Ga composition was measured in the divided areas of $2.0 \times 1.6 \text{ mm}^2$ by EDS.

with the (111)A plane.

Relative contributions of the solutal natural convection, and thermocapillary and solutal Marangoni convection to the melting process of a GaSb-InSb-GaSb system under 1g and μg conditions were also investigated numerically (Okano et al., 1991, 2003). The numerical simulation results show that thermocapillary convection enhances the melting near the free interface under both 1g and μg conditions. Under 1g conditions, the contribution of the solutal Marangoni convection to the flow field is less than that of the thermocapillary convection since the heavier component sinks to the lower part of the melt, and the concentration gradient on the free interface becomes very gentle. Consequently, the intensity of the solutal Marangoni convection is very small.

On the other hand, the interface shape is greatly affected by the presence of solutal Marangoni convection under μg condition, even though the velocity of the solutal Marangoni convection is relatively small.

6 Conclusions

A rich summary of author's typical research works over the last 40 years on interphase transport phenomena with interfacial fluid motion and

surface tension gradients (and related applications to single crystal growth and microgravity sciences) has been reported.

The interface mobility (i.e. an interfacial velocity caused by surface tension gradients induced by temperature or concentration gradients along the interface) is very important and affects the interphase transport phenomena.

A unified theory for momentum, heat and mass transfer on liquid-fluid and solid-fluid interfaces has been proposed with interface mobility taken into account. It has been shown that in such a theoretical framework, interfacial contamination and interfacial turbulence can be well explained, respectively, by suppression and enhancement of the interfacial velocity induced by surface tension gradients.

Transport phenomena on solid spheres, liquid drops and gas bubbles have been also treated in the context of the proposed theory. The theory has been also elaborated for crystal-melt and related melt-fluid interfaces.

The mechanisms underlying thermal and solutal Marangoni convection under gravity and microgravity conditions have been discussed and elucidated with the support of relevant microgravity experimental results.

For additional relevant and recent results the reader may consider the following works: Amberg and Shiomi (2005), Lappa (2005), Gelfgat et al. (2005), Lan and Yeh (2005), Tsukada et al. (2005), Li et al. (2006), Matsunaga and Kawamura (2006), El-Gamma and Floryan (2006), Okano et al. (2006), Ma and Walker (2006), Kaki-moto and Liu (2006), Sohail and Saghir (2006), Jaber and Saghir (2006), Giessler et al. (2005), Prud'homme and El Ganaoui (2007), Kamotani et al. (2007), Votyakov and Zienicke (2007).

Acknowledgement: The author would like to express sincere appreciation to all of coauthors and many students for their active works, and also to Japanese Government which supported many of these works, particularly, the Science and Technology Agency (presently, the Ministry of Economy, Trade and Industry) and the National Space Development Agency of Japan (presently, the Japan Aerospace Exploration Agency).

Nomenclature

| | | |
|----------|---|------------|
| A, A_S | aspect ratio, $A, A_S \equiv L/H$ | [-] |
| C_{fN} | modified friction coefficient when $u_s - u_\infty > 0$ | [-] |
| | $C_{fN} \equiv \tau_s / (\rho u_\infty (u_s - u_\infty) / 2)$ | |
| C_{DS} | drag coefficient of rigid spheres | |
| | $C_{DS} \equiv \tau_s / (\rho u_\infty^2 / 2)$ | [-] |
| D | diffusivity | $[m^2/s]$ |
| | or disk diameter | $[m]$ |
| d | crucible diameter | $[m]$ |
| Gr | Grashof number, $Gr \equiv g\beta\Delta T x^3 / \nu^2$ | [-] |
| H | melt depth | $[m]$ |
| h | heat transfer coefficient | $[W/m^2K]$ |
| I_0 | modified Bessele function | [-] |
| κ | mass transfer coefficient | $[m/s]$ |
| L | interface length | $[m]$ |
| Ma | Marangoni number | [-] |
| | $Ma \equiv (\partial\sigma/\partial x) \cdot x^2 / (\nu \cdot \mu)$ | |
| m | contamination degree, defined by Eq. (12) | [-] |
| Nu | Nusselt number, $Nu \equiv hx/\lambda$ | [-] |
| Pe | Peclet number, | [-] |
| | $Pe \equiv ux/\alpha$ (for heat transfer) | |
| | $Pe \equiv ux/D$ (for mass transfer) | |
| Pr | Prandtl number | [-] |
| | $Pr \equiv \nu/\alpha$ (for heat transfer) | |

| | | |
|------------|--|---------|
| R | radius | $[m]$ |
| Re | Reynolds number, $Re \equiv \rho ux/\mu$ | [-] |
| r | radial distance | $[m]$ |
| r_C | crystal radius | $[m]$ |
| Δr | length of melt interface | $[m]$ |
| Sc | Schmidt number, $Sc \equiv \mu/\rho D$ | [-] |
| Sh | Sherwood number, $Sh \equiv kx/D$ | [-] |
| T | temperature | $[K]$ |
| ΔT | temperature difference | $[K]$ |
| | between crucible wall and crystal, | |
| | or between both ends of liquid bridge | |
| t | time | $[s]$ |
| u | velocity parallel to interface | $[m/s]$ |
| u_T | terminal velocity | $[m/s]$ |
| V | liquid bridge volume | $[m^3]$ |
| V_0 | volume of cylindrical liquid bridge | $[m^3]$ |
| x | x^* coordinate | $[m]$ |

Greeks

| | | |
|------------|---|-------------------|
| α | thermal diffusivity | $[m^2/s]$ |
| κ | viscosity ratio, $\kappa \equiv \mu_d/\mu_c$ | [-] |
| λ | thermal conductivity | $[w/(m \cdot K)]$ |
| β | thermal expansion coefficient | $[1/K]$ |
| γ | density ratio, $\gamma \equiv \rho_d/\rho_c$ | [-] |
| μ | viscosity | $[Pa \cdot s]$ |
| σ | interfacial tension | $[N/m]$ |
| ν | kinematic viscosity, $\nu \equiv \mu/\rho$ | $[m^2/s]$ |
| ρ | density | $[kg/m^3]$ |
| θ | angle | $[radian]$ |
| τ_s | shear stress at stationary interface, | $[N/m]$ |
| | $\tau_s \equiv -\mu(\partial u/\partial y)_{y=0}$ | |
| ω | crystal rotation rate | $[radian/s]$ |
| ω^* | critical crystal rotation rate | $[radian/s]$ |
| | when crystal shape is plane | |

Subscripts

| | |
|------|--|
| c | continuous phase |
| $c+$ | positive critical point |
| $c-$ | negative critical point |
| d | dispersed phase |
| i | interface, or i th phase |
| init | initial |
| x | mass fraction |
| s | based on interfacial velocity, |
| | or stationary interface, or solid |
| w | water phase, which is rate-determining phase |

- ∞ free stream condition
 0 condition at $u_s = 0$
 1 1st phase
 2 2nd phase

References

- Amberg, G.; Shiomi, J.** (2005): Thermocapillary flow and phase change in some widespread materials processes. *FDMP: Fluid Dynamics & Materials Processing*, vol. 1, pp. 81-95.
- Arafune, K.; Hirata, A.** (1998): Interactive solutal and thermal Marangoni convection in a rectangular open boat. *Numerical Heat Transfer Part A: Applications*, vol. 34, no.4, pp. 421-429.
- Arafune, K.; Hirata, A.** (1999a): Thermal and solutal Marangoni convection in In-Ga-Sb system. *J. Crystal Growth*, vol. 197, no. 4, pp. 811-817.
- Arafune, K.; Kinoshita, A.; Fujiwara Y.; Hirata, A.** (2000): Characterization of oscillatory Marangoni convection in liquid bridges. *Proc. 51st Int. Astronaut. Cong.*, Paper No. IAF-00-J.4.02, pp. 1-7.
- Arafune, K.; Kodera, K.; Kinoshita, A.; Hirata, A.** (2003): Control of crystal-melt interface shape during horizontal Bridgman growth of InSb crystal using solutal Marangoni convection. *J. Crystal Growth*, vol. 249, no. 3-4, pp. 429-436.
- Arafune, K.; Sugiura, M.; Hirata, A.** (1999b): Investigation of steady Marangoni convection in low- and high- Prandtl number fluids. *J. Chem. Eng. Jpn.*, vol. 32, no.1, pp. 104-109.
- Arafune, K.; Yamamoto, K.; Hirata, A.** (2001): Interactive thermal and solutal Marangoni convection during compound semiconductor growth in a rectangular open boat. *Int. J. Heat and Mass Transfer*, vol. 44, no. 13, pp. 2405-2411.
- Azuma, H.; Yoshihara, S.; Ohnishi, M.; Hirata, A.; Nishizawa, S.; Yoshitomi, S.; Kawasaki, K.; Shirasu, H.** (1990): Liquid column formation by using drop tower. *Jpn. Soc. Microgravity Appl.*, vol. 7, no. 4, pp. 3-4.
- Berkowski, M.; Iliev, K.; Nikolov, V.; Peshev, P.; Piekarczyk, W.** (1987): On the conditions of formation of a flat crystal melt interface during Czochralski growth of single-crystals. *J. Crystal Growth*, vol. 83, no. 4, pp. 507-516.
- Berkowski, M.; Iliev, K.; Nikolov, V.; Peshev, P.; Piekarczyk, W.** (1991): Conditions of maintenance of a flat crystal melt interface during Czochralski growth of Bismuth Germanium oxide single-crystals. *J. Crystal Growth*, vol. 108, pp. 225-232.
- Brice, J. C.; Bruton, T. M.; Hill, O. F.; Whiffin, P. A. C.** (1974): The Czochralski growth of $\text{Bi}_{12}\text{SiO}_{20}$ crystals. *J. Crystal Growth*, vol. 24-25, pp. 429-431.
- El-Gamma, M.; Floryan, J. M.** (2006): Thermocapillary Effects in Systems with Variable Liquid Mass Exposed to Concentrated Heating. *FDMP: Fluid Dynamics & Materials Processing*, vol. 2, no. 1, pp. 17-26.
- Gelfgat, A. Yu.; Rubinov, A.; Bar-Yoseph, P. Z.; Solan, A.** (2005): On the Three-Dimensional Instability of Thermocapillary Convection in Arbitrarily Heated Floating Zones in Microgravity Environment. *FDMP: Fluid Dynamics & Materials Processing*, vol. 1, no. 1, pp. 21-32.
- Giessler, C.; Sievert, C.; Krieger, U.; Halbedel, B.; Huelsenberg, D.; Luedke, U.; Thess, A.** (2005): A Model for Electromagnetic Control of Buoyancy Driven Convection in Glass Melts. *FDMP: Fluid Dynamics & Materials Processing*, vol. 1, no. 3, pp. 247-266.
- Hayakawa, Y.; Balakrishnan, K.; Okano, Y.; Ozawa, T.; Kimura, T.; Komatsu, H.; Murakami, N.; Nakamura, T.; Arafune, K.; Koyama, T.; Miyazawa, M.; Hirata, A.; Imaishi, N.; Dost, S.; Dao, Le. H.; Kumagawa, M.** (2002): Experimental and numerical analysis of crystallization processes of $\text{In}_x\text{Ga}_{1-x}\text{Sb}$ under different gravity conditions. *J. Space Tech. Sci.*, vol. 15, no. 1, pp. 11-20.
- Hayakawa, Y.; Balakrishnan, K.; Shibata, N.; Komatsu, H.; Nakamura, T.; Murakami, N.; Yamada, T.; Krishnamurthy, D.; Koyama, T.; Ozawa, T.; Okano, Y.; Miyazawa, M.; Hirata, A.; Arafune, K.; Dost S.; Dao, Le. H.; Kumagawa, M.** (2001): Growth of InGaSb under reduced gravity using an airplane. *J. Jpn. Soc. Microgravity Appl.*, vol. 18, no. 2, pp. 79-83.
- Hayakawa, Y.; Okano, Y.; Ozawa, T.; Hirata,**

- A.; Arafune, K.; Imaishi, N.; Yamaguchi, T.; Kumagawa, M.** (2000): Experimental and numerical investigation on dissolution of GaSb into InSb melt under microgravity and terrestrial conditions. *J. Crystal Growth*, vol. 213, pp. 40-50.
- Hirata, A.** (1982): Behavior of single liquid drops. *Advances in Chem. Eng.*, no. 16, pp. 27-57. (in Japanese)
- Hirata, A.** (2005): Interphase transport phenomena and applications to microgravity science, single crystal growth, enzymatic synthesis process and biological wastewater treatment. *Proc. Int. Semi. Chem. Eng. Sci. Human Welfare, Waseda University*, pp. VIII 1-58.
- Hirata, A.; Arafune, K.; Fujiwara, S.; Kumagawa, M.; Hayakawa, Y.; Okitsu, K.; Imaishi, N.; Yasuhiro, S.; Okano, Y.; Sakai, S.; Osaka, T.; Yoda, S.; Oida, T.** (1996): Mixing of melt of multicomponent of compound semiconductor by solutal Marangoni convection. *J. Jpn. Soc. Microgravity Appl.*, vol. 13, no. 3, pp. 165-170.
- Hirata, A.; Arafune, K.; Suzuki, T.; Tanji, A.; Koyama, M.; Kawasaki, H.** (1997a): Observation of interactive Marangoni convection under various gravity fields. *J. Jpn. Soc. Microgravity Appl.*, vol. 14, Supplement, pp. 9-10.
- Hirata, A.; Kawakami M.; Okano, Y.** (1989): Effect of interfacial velocity and interfacial tension gradient on momentum heat and mass transfer. *Can. J. Chem. Eng.*, vol. 67, no. 10, pp. 777-786.
- Hirata, A.; Kira, K.; Suzuki, Y.** (1979a): Analysis of momentum and heat transfer through a moving interface with forced injection and suction. *J. Chem. Eng. Jpn.*, vol. 12, no. 6, pp. 474-477.
- Hirata, A.; Nishizawa, S.; Imaishi, N.; Okano, Y.; Saghir M. Z.; Scott, P. J.** (1991): Marangoni convection in a liquid bridge under earth gravity condition. *Proc. 42nd Cong. Int. Astronaut. Fed.*, Paper No. IAF-91-0907, pp. 1-7.
- Hirata, A.; Nishizawa, S.; Imaishi, N.; Yasuhiro, S.; Yoda, S.; Kawasaki, K.** (1993c): Oscillatory Marangoni convection in a silicone oil liquid bridge under microgravity by utilizing TR-IA sounding rocket. *J. Jpn. Soc. Microgravity Appl.*, vol. 10, no. 4, pp. 241-250.
- Hirata, A.; Nishizawa, S.; Noguchi, M.; Sakurai, M.; Yasuhiro, S.; Imaishi, N.** (1994): Marangoni convection in a liquid bridge under microgravity conditions during parabolic flight. *J. Chem. Eng. Jpn.*, vol. 27, no. 1, pp. 65-71.
- Hirata, A.; Nishizawa, S.; Okano, Y.** (1992a): Effect of interfacial tension gradient on momentum and mass transfer through a moving interface of single drops. *Solvent Extraction 1990, Proc. Int. Solvent Extraction Conf. (ISEC '90)*, Part A, pp. 841-846.
- Hirata, A.; Nishizawa, S.; Sakurai, M.** (1997b): Experimental results of oscillatory Marangoni convection in a liquid bridge under normal gravity. *J. Jpn. Soc. Microgravity Appl.*, vol. 14, no. 2, pp. 122-129.
- Hirata, A.; Nishizawa, S.; Sakurai, M.; Arafune, K.; Akiyama, T.; Imaishi, N.** (1993e): Interfacial contamination phenomena on Marangoni convection in a silicone oil liquid bridge. *J. Jpn. Soc. Microgravity Appl.*, vol. 10, no. 4, pp. 344-345.
- Hirata, A.; Nishizawa, S.; Sakurai, M.; Imaishi, N.** (1993d): Interfacial contamination caused by water on Marangoni convection in a silicone oil liquid bridge. *J. Chem. Eng. Jpn.*, vol. 26, no. 6, pp. 754-756.
- Hirata, A.; Okano, Y.** (1984): Mass transfer. *Kagaku Kogaku*, vol. 48, no. 4, pp. 236-243. (in Japanese)
- Hirata, A.; Okano, Y.; Yakushiji, K.; Harrison, B.** (1992c): The Czochralski process. *Advances in Transport Processes VIII* (Edited by Mujumdar, A. S.; Mashelkar, R. A.), Chapter 8, pp. 435-504, Elsevier Sci. Pub.
- Hirata, A.; Sakurai, M.; Ohishi, N.** (1997c): Effect of gravity on Marangoni convection in a liquid bridge. *J. Jpn. Soc. Microgravity Appl.*, vol. 14, no. 2, pp. 130-136.
- Hirata, A.; Sakurai, M.; Ohishi, N.; Koyama, M.; Morita, T.; Kawasaki, H.** (1997d): Transition process from laminar to oscillatory Marangoni convection in a liquid bridge under normal and microgravity. *J. Jpn. Soc. Microgravity Appl.*, vol. 14, no. 2, pp. 137-143.
- Hirata, A.; Shiotsuka, T.** (1967): A new

method for measuring instantaneous and local mass transfer rate. *Kagaku Kogaku*, vol. 31, no. 5, pp. 507-508. (in Japanese)

Hirata, A.; Suzuki, Y. (1980): High mass flux mass transfer through a mobile interface. *J. Chem. Eng. Jpn.*, vol. 13, no. 5, pp. 354-360.

Hirata, A.; Tachibana, M.; Okano, Y.; Fukuda, T. (1992b): Magnetic field effects on Marangoni and natural convections in a rectangular open boat. *J. Chem. Eng. Jpn.*, vol. 25, no. 1, pp. 62-66.

Hirata, A.; Tachibana, M.; Okano, Y.; Fukuda, T. (1993a): Observation of crystal-melt interface shape in simulated Czochralski method with model fluid. *J. Crystal Growth*, vol. 128, pp. 195-200.

Hirata, A.; Tachibana, M.; Sugimoto, T.; Okano, Y.; Fukuda, T. (1993b): Control of crystal-melt interface shape during growth of lithium niobate single crystal. *J. Crystal Growth*, vol. 131, pp. 145-152.

Hirayama, H.; Ainoya, M.; Kinoshita, A.; Hirata, A.; Aoyagi, Y. (2001a): Drastic reduction of threading dislocation density of AlGa_N on SiC wafer by using highly-Si-incorporated AlGa_N superlattice. *MRS Int. J. Nitride Semicond. Res.*, vol. 639, no. G1.3, pp. 1-6.

Hirayama, H.; Enomoto, Y.; Kinoshita, A.; Hirata, A.; Aoyagi, Y. (2000a): Optical properties of AlGa_N quantum well structures. *MRS Int. J. Nitride Semicond. Res.*, vol. 595, no. W11.35, pp. 1-6.

Hirayama, H.; Enomoto, Y.; Kinoshita, A.; Hirata, A.; Aoyagi, Y. (2000b): 230 to 250 nm intense emission from AlN/AlGa_N quantum wells. *Phys. Stat. Sol. A*, vol. 180, no. 1, pp. 157-161.

Hirayama, H.; Enomoto, Y.; Kinoshita, A.; Hirata, A.; Aoyagi, Y. (2002): Efficient 230-280 nm emission from high-Al-content AlGa_N-based multiquantum wells. *Appl. Phys. Lett.*, vol. 80, no. 1, pp. 37-39.

Hirayama, H.; Kinoshita, A.; Yamanaka, T.; Hirata, A.; Aoyagi, Y. (2001b): In segregation effects on optical and doping properties of InAlGa_N for UV emitting devices. *MRS Int. J. Nitride Semicond. Res.*, vol. 639, no. G2.8, pp. 1-6.

Jaber, T. J.; Saghir, M. Z. (2006): The Effect of Rotating Magnetic Fields on the Growth of SiGe Using the Traveling Solvent Method. *FDMP: Fluid Dynamics & Materials Processing*, vol. 2, no. 3, pp. 175-190.

Kakimoto, K.; Liu, L. (2006): Flow instability of silicon melt in magnetic fields. *FDMP: Fluid Dynamics & Materials Processing*, vol. 2, no. 3, pp. 167-174.

Kamotani, Y.; Matsumoto, S.; Yoda, S. (2007): Recent developments in oscillatory Marangoni convection, *FDMP: Fluid Dynamics & Materials Processing*, vol. 3, no. 2, pp. 147-160.

Kinoshita, A.; Arafune, K.; Sakurai, M.; Yamada, A.; Hirata, A. (2001b): Clarification of flow structure of the time-dependent Marangoni convection in silicone-oil liquid-bridges. *Proc. 2nd Pan Pacific Basin Workshop on Microgravity Sci. 2001.*, no. IF-1063, pp. 1-10.

Kinoshita, A.; Hirayama, H.; Ainoya, M.; Hirata, A.; Aoyagi, Y. (2000b): Room-temperature operation at 333 nm of Al_{0.03}Ga_{0.97}N/Al_{0.25}Ga_{0.75}N quantum-well light-emitting diodes with Mg-doped superlattice layers. *Appl. Phys. Lett.*, vol. 77, no. 2, pp. 175-117.

Kinoshita, A.; Hirayama, H.; Ainoya, M.; Yamabi, T.; Hirata, A.; Aoyagi, Y. (2001a): Current injection UV- emission from InAlGa_N multi quantum well light-emitting diodes. *MRS Int. J. Nitride Semicond. Res.*, vol. 639, no. G12.6, pp. 1-6.

Kinoshita, A.; Hirayama, H.; Kim, J. S.; Ainoya, M.; Hirata, A.; Aoyagi, Y. (2000c): Current injection emission at 333 nm from Al_{0.03}Ga_{0.97}N/Al_{0.25}Ga_{0.75}N multi quantum well ultraviolet light emitting diodes. *Phys. Stat. Sol. A*, vol. 180, no. 1, pp. 397-401.

Kinoshita, A.; Hirayama, H.; Riblet, P.; Ainoya, M.; Hirata, A.; Aoyagi, Y. (2000a): Emission enhancement of GaN/AlGa_N single-quantum-wells due to screening of piezoelectric field. *Int. J. Nitride Semicond. Res.*, vol. 595, no. W11-32, pp. 1-6.

Lan, C. W.; Yeh, B.C. (2005): Effects of rotation on heat flow, segregation, and zone shape in a

small-scale floating-zone silicon growth under axial and transversal magnetic fields. *FDMP: Fluid Dynamics & Materials Processing*, vol. 1, no. 1, pp. 33-44.

Lappa, M. (2005): Review: Possible strategies for the control and stabilization of Marangoni flow in laterally heated floating zones. *FDMP: Fluid Dynamics & Materials Processing*, vol. 1, no. 2, pp. 171-188.

Li, Y. R.; Peng, L.; Shi, W. Y.; Imaishi, N. (2006): Convective instability in annular pools. *FDMP: Fluid Dynamics & Materials Processing*, vol. 2, no. 3, pp. 153-166.

Lukasiewicz, T.; Majchrowski, A. (1992): Czochralski growth of TeO₂ single-crystals under conditions of forced- convection in the melt. *J. Crystal Growth*, vol. 116, no. 3-4, pp. 364-368.

Ma, N.; Walker, J. S. (2006): Electromagnetic Stirring in Crystal Growth Processes. *FDMP: Fluid Dynamics & Materials Processing*, vol. 2, no. 2, pp. 119-126.

Matsunaga, K.; Kawamura, H. (2006): Influence of Thermocapillary Convection on Solid-liquid Interface. *FDMP: Fluid Dynamics & Materials Processing*, vol. 2, no. 1, pp. 59-64.

Meguro, T.; Iwai, S.; Aoyagi, Y.; Ozaki, K.; Yamamoto, Y.; Suzuki, T.; Okano, Y.; Hirata, A. (1990b): Atomic layer epitaxy of AlAs and Al-GaAs. *J. Crystal Growth*, vol. 99, pp. 540-544.

Meguro, T.; Iwai, S.; Aoyanagi, Y.; Suzuki, T.; Hirata, A. (1990a): Effect of simultaneous thermal pulse and laser irradiation on atomic monolayer epitaxy of GaAs. *Kagaku Kogaku*, vol. 16, no. 3, pp. 620-623. (in Japanese)

Meguro, T.; Suzuki, T.; Ozaki, K.; Okano, Y.; Hirata, A.; Yamamoto, Y.; Iwai, S.; Aoyagi, Y.; Namba, S. (1988): Surface processes in laser-atomic layer epitaxy (Laser-ALE) of GaAs. *J. Crystal Growth*, vol. 93, pp. 190-194.

Miller, D. C.; Valentino, A. J.; Shick, L. K. (1978): The effect of melt flow phenomena on the perfection of Czochralski grown gadolinium gallium garnet. *J. Crystal Growth*, vol. 44, no. 2, pp. 121-134.

Miyazawa, S. (1980): Fluid-flow effect on gas-

bubble entrapment in Czochralski-grown oxide crystals. *J. Crystal Growth*, vol. 49, no. 3, pp. 515-521.

Miyazawa, S.; Kondo, S. (1973): Preparation of paratellurite TeO₂/2. *Mater. Res. Bull.*, vol. 8, no. 10, pp. 1215-1221.

Miyazawa, Y.; Mori, Y.; Homma, S. (1978): Interface shape transitions in the Czochralski growth of Dy₃Al₅O₁₂. *J. Crystal Growth*, vol. 43, pp. 541-542.

Miyazawa, Y.; Mori, Y.; Homma, S.; Kitamura, K. (1978): Interface shape transition in Czochralski grown YAG crystals. *Mater. Res. Bull.*, vol. 13, no. 7, pp. 675-680.

Okano, Y.; Ishii, A.; Miyashita, H.; Minakuchi, H.; Dost, S. (2006): A numerical study of controlling the g-jitter induced convection in the solution of a crystal growth crucible under microgravity. *FDMP: Fluid Dynamics & Materials Processing*, vol. 2, no. 4, pp. 261-270.

Okano, Y.; Fukuda, T.; Hirata, A.; Takano, N.; Tsukada, T.; Hozawa, M.; Imaishi, N. (1991): Numerical study on Czochralski growth of oxide single crystal. *J. Crystal Growth*, vol. 109, pp. 94-98.

Okano, Y.; Hatano, A.; Hirata, A. (1989b): Natural and Marangoni convections in a floating zone. *J. Chem. Eng. Jpn.*, vol. 22, no. 4, pp. 385-388.

Okano, Y.; Itoh, M.; Hirata, A. (1989a): Natural and Marangoni convections in a two-dimensional rectangular open boat. *J. Chem. Eng. Jpn.*, vol. 22, no. 3, pp. 275-281.

Okano, Y.; Shimizu, J.; Hayakawa, Y.; Kumagawa, M.; Hirata, A.; Dost, S. (2003): A numerical study for the role of natural convection in the melting of an GaSb/InSb/GaSb sandwich system. *Numerical Heat Transfer, Part A*, vol. 43, no. 1, pp. 31-46.

Okano, Y.; Tachibana, M.; Hatano, A.; Hirata, A. (1989c): Control of crystal-melt interface shape during Czochralski growth of oxide single crystals. *J. Chem. Eng. Jpn.*, vol. 22, no. 4, pp. 389-394.

Okano, Y.; Umemura, S.; Enomoto, Y.;

- Hayakawa, Y.; Kumagawa, M.; Hirata, A.; Dost, S.** (2002): Numerical study of Marangoni convection effect on the melting of GaSb/InSb/GaSb. *J. Crystal Growth*, vol. 235, no. 1-4, 135-139.
- Okitsu, K.; Hayakawa, Y.; Hirata, A.; Fujiwara, S.; Okano, Y.; Imaishi, N.; Yoda, S.; Oida, T.; Yamaguchi, T.; Kumagawa, M.** (1996): Gravitational effects on mixing and growth morphology of an $\text{In}_{0.5}\text{Ga}_{0.5}\text{Sb}$ system. *J. Cryst. Res. Technol.*, vol. 31, no. 8, pp. 969-978.
- Okitsu, K.; Hayakawa, Y.; Yamaguchi, T.; Hirata, A.; Fujiwara, S.; Okano, Y.; Imaishi, N.; Yoda, S.; Oida, T.; Kumagawa, M.** (1997): Melt mixing of the $0.3\text{In}/0.7\text{GaSb}/0.3\text{Sb}$ solid combination by diffusion under microgravity. *Jpn. J. Appl. Phys.*, vol. 36, pp. 3613-3619.
- Okitsu, K.; Hayakawa, Y.; Yamaguchi, T.; Kumagawa, M.; Hirata, A.; Tachibana, M.; Imaishi, N.** (1994): Preliminary experiment on the earth for InGaSb growth under microgravity and numerical analysis of nucleus generation. *Advanced Materials '93, 1A: Computations, Glassy Materials, Microgravity and Non-Destructive Testing*, Ed. by Masumoto T. et al., *Trans. Mat. Res. Soc. Jpn.*, vol. 16A, pp. 691-694.
- Ozawa, T.; Hayakawa, Y.; Okano, Y.; Adachi, H.; Morio, N.; Balakrishnan, K.; Yamaguchi, T.; Miyazawa, M.; Hirata, A.; Imaishi, N.; Dao, L. H.; Kumagawa, M.** (2000): Numerical simulations for dissolution processes of InGaSb semiconductors. *Advances in Computational Eng. Sci.*, vol. 1, pp. 328-333.
- Ozawa, T.; Hayakawa, Y.; Okano, Y.; Ori, K.; Adachi, H.; Murakami, N.; Balakrishnan, K.; Miyazawa, M.; Hirata, A.; Imaishi, N.; Kumagawa, M.** (2001): Effect of gravity force on the dissolution process of GaSb into InSb melt. *Advances in Computational Eng. Sci.*, vol. 1, pp. 1-8.
- Preisser, F.; Schwabe, D.; Scharmann, A.** (1983): Steady and oscillatory thermocapillary convection in liquid columns with free cylindrical surface. *J. Fluid Mech.*, vol. 126, pp. 545-567.
- Prud'homme, R.; El Ganaoui, M.** (2007): Solid/Liquid Phase Change: Recent Studies and Models. *FDMP: Fluid Dynamics & Materials Processing*, vol. 3, no. 2, pp. 161-172.
- Saitou, M.; Hirata, A.** (1991a): Numerical methods for solving unsteady solidification problems. *Simulation*, vol. 10, no. 4, pp. 315-321. (in Japanese)
- Saitou, M.; Hirata, A.** (1991b): Numerical method for unsteady solidification problems with melt flow. *10th Simulation Technol. Conf.*, pp. 15-18. (in Japanese)
- Saitou, M.; Hirata, A.** (1991c): Numerical calculation of two-dimensional unsteady solidification problem. *J. Crystal Growth*, vol. 113, pp. 147-156.
- Saitou, M.; Hirata, A.** (1992a): Two-dimensional unsteady solidification problem calculated by using the boundary fitted coordinate system. *J. Comput. Phys.*, vol. 100, pp. 188-196.
- Saitou, M.; Hirata, A.** (1992b): Ratio of liquid to solid thermal conductivity calculated from the solid-liquid interface shape. *J. Crystal Growth*, vol. 118, pp. 365-370.
- Saitou, M.; Hirata, A.** (1992c): Numerical solution of the unsteady solidification problem with a solute element by using the boundary-fitted coordinate system. *Numer. Heat Trans., Part B*, vol. 22, pp. 63-77.
- Saitou, M.; Hirata, A.** (1993): A numerical method for solving the two-dimensional unsteady solidification problem with the motion of melt by using the boundary-fitted co-ordinate system. *Int. J. Numer. Method Eng.*, vol. 36, pp. 403-416.
- Sakurai, M.; Ohishi, N.; Hirata, A.** (1999): Oscillatory thermocapillary convection features in a liquid bridge under normal gravity and microgravity conditions. -drop shaft experiments- *Advance Space Res.*, vol. 24, no. 10, pp. 1379-1384.
- Shirotsuka, T.; Hirata, A.** (1967): Heat and mass transfer through shock tube wall boundary layer. *JSME 1967 Semi-Int. Sympo.*, Paper No. 218, pp. 145-153.
- Shirotsuka, T.; Hirata, A.** (1970): A new method for measuring instantaneous and local

mass transfer rate. *J. Chem. Eng. Jpn.*, vol. 3, no. 2, pp. 176-181.

Shirotsuka, T.; Hirata, A. (1971a): Continuous phase mass transfer from single liquid drops in liquid-liquid system. *Kagaku Kogaku*, vol. 35, no. 1, pp. 78-84. (in Japanese)

Shirotsuka, T.; Hirata, A. (1971b): Continuous phase mass transfer from single gas bubbles in gas-liquid system. *Kagaku Kogaku*, vol. 35, no. 1, pp. 123-124. (in Japanese)

Shirotsuka, T.; Hirata, A.; Murakami, A. (1966): *Rate theory on transport phenomena for chemical engineer*. Ohm co. Ltd. (in Japanese)

Shirotsuka, T.; Hirata, A.; Niwa, J. (1972): Interphase mass transfer with a flowing interface between the two-laminar immiscible liquid layers. *Kagaku Kogaku*, vol. 36, no. 12, pp. 1314-1320. (in Japanese)

Shirotsuka, T.; Hirata, A.; Sakai, K. (1969): Analysis of unsteady-state mass transfer through an interface between different phases. the case of varying surface concentration accompanying interfacial flow. *Int. Chem. Eng.*, vol. 9, no. 3, pp. 546-553. and *Kagaku Kogaku*, vol. 33, no. 2, pp. 168-174.

Simko, J. P.; Meguro, T.; Iwai, S.; Ozasa, K.; Hirata, A.; Aoyagi, Y.; Sugano, T. (1992): Direct observation of self-limiting gallium deposition on GaAs during laser-atomic layer epitaxial processing. *Jpn. J. Appl. Phys.*, vol. 31, Part 2 (11A), pp. L1518-L1521.

Sohail, M.; Saghri, M. Z. (2006): Three-Dimensional Modeling of the Effects of Misalignment on the Growth of Ge_{1-x}Si_x by The Traveling Solvent Method. *FDMP: Fluid Dynamics & Materials Processing*, vol. 2, no. 2, pp. 127-140.

Tachibana, M.; Hirata, A.; Okano, Y.; Fukuda, S. (1990): Interfacial phenomenon on molten surface of oxide. *Nihon Kesyō Seicho Gakkai*, vol. 17, no. 3&4, pp. 323-329. (in Japanese)

Takagi, K.; Fukazawa, T.; Ishii, M. (1976): Investigation of the direction of the solid-liquid interface on the Czochralski grown of GGG crystals. *J. Crystal Growth*, vol. 32, no. 1, pp. 89-94.

Thorsen, G.; Stordalen, R. M.; Terjesen, S. G. (1968): On the terminal velocity of circulating and oscillating liquid drops. *Chem. Eng. Sci.*, vol. 23, pp. 413-426.

Thorsen, G.; Terjesen, S. G. (1962): On the mechanism of mass transfer in liquid-liquid extraction. *Chem. Eng. Sci.*, vol. 17, pp. 137-148.

Trauth, J.; Grabmaier, B. C. (1991): The shape of the crystal melt interface during the growth of Lithium-Niobate crystals by the Czochralski technique. *J. Crystal Growth*, vol. 112, no. 2-3, pp. 451-457.

Tsukada, T.; Kobayashi, M.; Jing, C. J.; Imaishi, N. (2005): Numerical simulation of CZ crystal growth of oxide. *FDMP: Fluid Dynamics & Materials Processing*, vol. 1, no. 1, pp. 45-62.

Votyakov, E. V.; Zienicke, E. A. (2007): Numerical Study of Liquid Metal Flow in a Rectangular Duct under the Influence of a Heterogeneous Magnetic Field. *FDMP: Fluid Dynamics & Materials Processing*, vol. 3, no. 2, pp. 97-114.

Yao, Y. L.; Shu, J. Z.; Xie, J. C.; Hu, W. R.; Hirata, A.; Nishizawa, S.; Sakurai, M. (1997): Transition of oscillatory floating half zone convection from earth's gravity to microgravity. *Int. J. Heat and Mass Transfer*, vol. 40, no. 11, pp. 2517-2524.

Yasuhiro, S.; Sato, T.; Imaishi, N.; Hirata, A.; Kumagawa, M. (1997): Numerical simulation of solutal Marangoni convection during liquid mixing under microgravity. *Microgravity Sci. Technol.*, vol. 4, no. 4, pp. 237-244.

Yoshitomi, S.; Naki, M.; Sugawara, M.; Hirata, A.; Nishizawa, S.; Noguchi, M.; Sakurai, M.; Imaishi, N.; Yasuhiro, S.; Kawasaki, K.; Masuda, T.; Muramatsu, S. (1992): Development of equipment and preliminary experiment for sounding rocket experiment, TR-1A sounding rocket. -investigation of creation and control of Marangoni convections- *Parabolic Flight*, vol. 2, no. 1, pp. 33-39.